Salicaceae endophyte inoculation alters stomatal patterning and improves the intrinsic water use efficiency of *Populus trichocarpa*

Matthew Hendrickson

A thesis

submitted in partial fulfillment of the

requirements for the degree of

Master of Science

University of Washington

2023

Committee:

Soo-Hyung Kim

Sharon Doty

Jonathan D. Bakker

Program Authorized to Offer Degree:

School of Environmental and Forest Sciences

University of Washington

Abstract

Salicaceae endophyte inoculation alters stomatal patterning and improves the intrinsic water use efficiency of *Populus trichocarpa*

Matthew Hendrickson

Chair of the Supervisory Committee:
Soo-Hyung Kim
School of Environmental and Forest Sciences

Background and Aims

Microorganisms may symbiotically enhance plant resilience to water stress by altering their hosts' physiology and anatomy at the leaf level. Bacterial and yeast endophytes, isolated from the Salicaceae family, can improve the intrinsic water use efficiency (*iWUE*) of cultivated poplar (*Populus*) under water deficits by lowering stomatal conductance (g_{sw}) while maintaining carbon assimilation (A_{net}). However, the relevance of stomatal anatomy underlying the reductions in g_{sw} remains unclear, and examining these traits may illuminate the way endophytes boost host acclimation to water stress. We hypothesized that endophyte inoculation could change host stomatal anatomy, and this would relate to decreases in g_{sw}.

Methods

In two greenhouse studies, we subjected Salicaceae endophyte-inoculated and uninoculated *Populus trichocarpa* to well-watered and water-deficit treatments. We examined the changes of

individual stomatal traits and related the composition of these parameters, termed stomatal patterning, to leaf-gas exchange under light saturation.

Key Results

Regardless of soil moisture status, inoculation improved *iWUE* at light saturation in experiment I from preserving A_{net} and lowering g_{sw}; however, increases in *iWUE* were more pronounced during the water deficit. Drops in g_{sw} corresponded to underlying shifts in stomatal patterning, and inoculated plants tended to have smaller, more compact stomata and greater anatomical maximum stomatal conductance (g_{smax}) relative to the control. Experiment II resulted in no changes in stomatal morphology from inoculation.

Conclusions

Our results indicate that inoculation with Salicaceae endophytes can alter stomatal density and size relationships, leading to lower g_{sw} and greater *iWUE*. However, improving the water-use efficiency of cultivated plants through endophytes likely relies on successful colonization of the host which may depend on the context of environmental conditions. Future efforts may quantify specific strains to examine a direct relationship between endophytes and host physiology and anatomy.

Table of contents

List of figures

List of tables

Acknowledgements

I would like to express my sincerest gratitude to my advisor, Professor Soo-Hyung Kim, for his wisdom, patience, and encouragement during my time in school. His gentle guidance instilled humility, creativity, and curiosity, and I hope to carry these qualities everywhere I go in life.

Thank you to my committee members, Professor Sharon Doty and Professor Jon Bakker, for their insight, time, and support during this work. Professor Doty's kindness and positivity set a great example of resilience during this research, and Professor Bakker's excellent teaching helped me understand nuanced data analysis.

Thank you to all current and former members of the Plant Ecophysiology and Modeling Lab: Professor Kyungdahm Yun, Dr. Darshi Banan, Dr. Beomseok Seo, Dr. Sun Woo Chung, Amelia Keyser-Gibson, Allison Fron, Arthur Hsin-Wu Hsu, Jane Callagan, Leah Valentine, Jun Hyuk Jeon, Miro Stuke, Sabrina Zerrade, Shubroto Sarkar, Sriram Parasurama, Vivian Corcoro, and Zohar Kolodner. I have enjoyed all our lab hangouts and conversations throughout the years. Every member has helped me get to this point, and I would like to give a special thanks to Darshi - I am indebted to his help, and I appreciate the calm, steady mentorship as I navigated the uncertainties of graduate school.

Thank you to the collaborators from the Doty Lab and Pacific Northwest National Laboratory who made long days in the field enjoyable, and to the University of Washington Botanical Garden staff for helping maintain the greenhouse for our experiments.

Also, a special thanks to the ESRM 499 students, that collected data and gave me the opportunity to help guide their independent research projects. With their help, no stomata were left behind.

This research was supported by the DOE Office of Science, Biological and Environmental Research (BER) Program through grant DE-SC0021137, and I am obliged to the funding that gave me the opportunity to explore my research interests.

Finally, I am grateful for my family, friends, and partner for their endless love and support in anything I do. Thank you for your care during the stress, guidance through the unexpected, solace from my failures, and shared happiness for my successes.

1 Introduction

Climate change is extending regional droughts, threatening the sustainable productivity of vulnerable forest systems (IPCC 2023; Vose et al. 2016). To preserve stand growth without increasing irrigation, silviculture industries can improve the water-use efficiency (*WUE*) of trees (Stenzel et al., 2021). *WUE* represents the ratio of carbon gained for biomass to water lost, and this concept applies to different spatial scales, ranging from entire ecosystems to individual plant leaves (Hatfield & Dold, 2019). At the leaf-level, *WUE* describes two separate processes: extrinsic *WUE* (abbreviated still as *WUE*) and intrinsic *WUE* (*iWUE*). While both models assess the net instantaneous rate of leaf carbon assimilation (A_{net}), *WUE* divides this term by leaf transpiration (*E*) whereas *iWUE* uses the stomatal conductance to water vapor (g_{sw}). This subtle difference implies that *WUE* (A_{net} /*E*) takes environmental variables into account through the calculation of *E* (e.g., vapor pressure deficit), whereas *iWUE* (A_{net}/g_{sw}) relies solely on the inherent physiology of a species (Rho & Kim, 2017).

Commercially and ecologically valuable trees, such as black cottonwood (*Populus trichocarpa)*, are susceptible to water stress, and increasing *WUE* remains a target to maintain their yields (Marron et al., 2014). While refining the *WUE* of these trees has relied on genomic-assisted breeding, this approach is slow due to *Populus* reproduction rates compared to environmental change (Stanton et al., 2014; Biselli et al., 2022). To supplement this process, induced acclimation can leverage the phenotypic plasticity of plant leaves to modify *iWUE* (Flexas et al., 2013, Leakey et al., 2019). Advancing *iWUE* depends on the stomatal pores embedded in the leaf epidermis, which link the intercellular space to the environment. Functionally, these openings balance the exchange of internal water vapor loss with aerial carbon assimilation by responding to external and inner signals (Harrison et al., 2019; Buckley 2019).

Plants control this gaseous tradeoff by dynamically shifting the aperture of existing pores or developmentally altering their size, number, and distribution in newly emergent leaves (Lawson et al., 2014).

Stomatal adjustments can influence several other physiological aspects, such as evaporative leaf cooling (Urban et al., 2017), mass-flow nutrient uptake (He & Dijkstra, 2014), or biomass accumulation (Alfas et al., 2006). Consequently, interspecific adaptations of stomatal traits to a prolonged drought evokes a cost-benefit effect, incurring a biological gain at the expense of another (Muir, 2015; de Boer et al., 2016; Mckown et al., 2019). This presents a challenge to boost *iWUE* of cultivated trees like black cottonwood that may inherently tailor stomatal patterning to maximize growth rates instead of water conservation under dry conditions (Dunlap & Stettler, 2001; Pearce et al., 2006; Mckown et al., 2014, 2019). Therefore, refining *iWUE* in poplars may require innovative methods, and one flexible strategy applies the mutualistic partnership between plants and microorganisms (Doty et al., 2017; Rho et al., 2018c).

Naturally, a plant and its microbiome form a unique holobiont, or discrete ecological unit, coadapted to a specific environment (Vandenkoornhuyse et al., 2015). In its native riparian habitat along the North American Cascade Range, black cottonwood carries distinct strains of endophytes – microbes that live inside plants - that vary with climatic locations (Fircinelli et al., 2020; Doty et al., 2009). Select bacterial endophytes assist black cottonwood within its nutrient poor soils by fixing dinitrogen gas in return for photosynthates or inorganic acids (Doty et al. 2016; Rho et al., 2018a; Kandel et al. 2017). Isolating these strains, along with others from the Salicaceae family, and inoculating different plant species provides diverse host benefits such as greater biomass, seedling viability, and improved water relations (Kahn et al., 2012; Aghai et al., 2019, Rho et al., 2018c; Rho et al. 2020a). While endophytes offer plant growth promotion

(PGP) and resilience imposed by water stresses, an effect on a particular PGP mechanism depends highly on specific contexts (Rho et al., 2018b). Replicating experimental conditions to examine the impact of a host-strain symbiosis on a process has led to different outcomes due to the complexity of plant-microbe-environment interactions (Rho & Kim, 2017).

In black cottonwood, inoculation with Salicaceae endophytes have shown to maintain A_{net} under a water-deficit while decreasing g_{sw} around midday, improving *iWUE* (Banan et al., 2023). Other water-stress experiments in additional species such as hybrid poplar (Kahn et al., 2016), and rice (Rho et al., 2018c) have revealed comparable results – the latter attributing it partly to decreases in abaxial stomatal density. However, under different stresses, endophytes from this consortium show no effect on g_{sw} (Knoth et al., 2014; Rho et al., 2020a, Rho et al., 2020b), and the greater literature details diverse outcomes on g_{sw} based on diverging mechanisms (Rho & Kim 2017). Variation of this highly dynamic parameter across studies encourages an examination of the morphological traits that underly its physiology.

Plants may identify beneficial endophytes through microbe-associated molecular patterns (MAMPs) as a part of innate immunity (Carvalho et al. 2016). Although the connection between MAMPs and stomatal closure has received extensive study through the concept of stomatal defense, the importance of these signals on stomatal development needs further investigation (reviewed in Melotto et al., 2017). Microbes can interact with a plant through immune receptors, secondary messengers, and hormones. For instance, Salicaceae endophytes can generate plant hormones (Khan et al., 2016), and have shown to increase abscisic acid (ABA) concentration in leaf tissue (Rho et al., 2018c) – a crucial regulator of stomatal dynamics and development. While a theory exists of pathogenic influence on leaf-gas exchange via shifts in stomatal morphology

(Muir 2020), the empirical relationship of commensal endophytes on these mechanisms remains unclear. In particular, the extent of PGP endophytes on the anatomical stomatal traits underlying g_{sw} has received little attention (Rho et al., 2018c; Rho et al. 2020b). This study attempted to determine the impact of Salicaceae endophytes on stomatal morphology in black cottonwood and relate it to its leaf gas-exchange during a water-deficit.

1.1 Research Questions and Hypotheses

We performed two separate factorial greenhouse experiments to determine the influence of endophyte inoculation on the gas exchange and stomatal patterning of black cottonwood under water stress. We defined stomatal patterning as the multivariate set of anatomical stomatal traits. The goal was to characterize the changes in leaf stomatal anatomy from inoculation with specific endophyte strains that could explain previously observed responses in g_{sw} and *iWUE* during a water-deficit (Rho et al., 2018c; Kahn et al., 2016; Banan et al., 2023). The rationale for the hypotheses was based on the understanding that some of the Salicaceae endophytes produce hormones that crosstalk in stomatal development, particularly ABA (Kahn et al., 2016, Rho et al., 2018c). Therefore, the hypotheses were to determine whether inoculation of *Populus trichocarpa* with specific Salicaceae endophytes would do the following before and after a water-deficit: (1) lower operational g_{sw} while maintaining the maximum assimilation rate under high light (A_{max}; 2000 $\mu mol_{photons}\, m^{-2}\, s^{-1}$) , (2) change the trends of stomatal patterning (**Table 1**) that would result in (3) accumulated differences in stomatal patterning, and (4) coordinate operational g_{sw} with stomatal patterning.

Table 1. List of parameters referenced within text and the accompanying units. Each stomatal trait contains a prefix of *Ad* or *Ab* to correspond it to either the adaxial (upper) or abaxial (lower) leaf surface, respectively. Shaded cells represent variables that encompass stomatal patterning (i.e., composition of stomatal traits); unshaded cells indicate leaf gas-exchange parameters.

Parameter	Definition	Units
GCL	Guard cell length. Distance of the stomatal complex on the major axis from the outermost edges of the guard cells.	µm
g_{smax}	Maximum anatomical stomatal conductance. Latent variable determined from geometric assumptions that describes the greatest conductance based on anatomy.	mol m^{-2} s^{-1}
PL	Pore length. Distance of the stomatal pore on the major axis from the innermost edges of the guard cells.	µm
PW	Pore width. Distance of the stomatal pore on the minor axis from the innermost edges of the guard cells.	µm
SD	Stomatal density. Number of stomata per unit area.	mm^{-2}
SI	Stomatal index. Number of stomata per total number of epidermal cells (pavement cells + stomata).	-
SR	Stomatal ratio. Number of adaxial stomata per abaxial stomata.	-
α	Apparent photochemical efficiency	µmol CO_2 mol^{-1}_{photon}
A_{max}	Light saturated A_{net} at ambient [CO_2] at 25 ^oC	µmol m^{-2} s^{-1}
A_{net}	Net CO_2 assimilation rate.	µmol m^{-2} s^{-1}
E	Transpiration, or water lost through stomata in response to enviro	mol m^{-2} s^{-1}
g_{sw}	Stomatal conductance to water vapor.	mol m^{-2} s^{-1}
iWUE	Intrinsic water-use efficiency. Leaf-level trait that describes the ratio of A_{net} to g_{sw}	µmol mol^{-1}
R_d	Leaf mitochondrial respiration at 25 ^oC	µmol m^{-2} s^{-1}
WUE	Extrinsic water-use efficiency. Leaf-level trait that describes the ratio of A_{net} to E	µmol mol^{-1}

2 Methods

Two controlled experiments were performed in the greenhouse of the Douglas Research Conservatory at the Center of Urban Horticulture, located at the University of Washington. Both experiments are detailed below and **Table 3** summarizes the key differences.

Endophyte origin and inoculum preparation

Two separate consortia were created from fifteen endophyte strains isolated from *Populus* and *Salix* species growing in nitrogen-limited, sandy cobblestone soils that experience cyclic flooding from alpine snow melt (**Table 2**). The first consortium, termed "DOE mix," was used in both experiment I and II. Consortium two, named "Yakima River mix," was only used in experiment II. Strains from the DOE mix were selected based on their ability to improve productivity and drought tolerance in a variety of previous hosts (Khan et al., 2012, 2015, 2016 Knoth et al., 2013, 2014; Kandel et al., 2015; Rho et al., 2018c). These were isolated from species that experience an oceanic climate on the West side of the Cascade Range. Strains from the Yakima River mix were isolated from *Populus* located in a xeric climate on the East side of the Cascade Range, near Ellensburg, Washington, that shows distinct leaf phenotypes relative to *Populus* from mesic sites (Dunlap & Stettler, 2001).

Preparation of the inoculum shared similar protocols as previous articles (Banan et al., 2023; Kahn et al., 2016). Briefly, each strain was grown in 10 ml MG/L broth (Cangelosi et al. 1991) and incubated at 30°C overnight while shaking. Cells were harvested with centrifugation at 6000 rpm at 4°C for 10 minutes before resuspension in 2 ml of nitrogen free media (NFM; Doty et al., 2009). Cell densities of each strain were diluted with NFM to an optical density (OD600) of 0.1 before mixing with equal volumes to generate an inoculum with an overall OD600 of 0.1.

Table 2. List of endophyte strains used in the experiments and its membership within a consortium. Endophytes included in the DOE consortium were isolated from trees on the Westside of the Cascade Range; strains isolated from the Yakima River consortium (YR) were isolated from species along the east side of the Cascades. The closest taxonomic classification is given from 16S rRNA sequencing.

Strain	Closest rRNA match	Host source	Reference
DOE Consortium			
PTD1	*Rhizobium sp.*	Snoqualmie River *P. trichocarpa x deltoides* branch	Doty et al. 2005
R10	*Rahnella sp.*	Skykomish River *P. trichocarpa* root	Doty et al. 2009
SD1	*Azotobacter sp.*	Skykomish River *P. trichocarpa* root	This experiment
SD2	*Azospirillium sp.*	Skykomish River *P. trichocarpa* root	This experiment
WP1	*Rhodotorula graminis*	Snoqualmie River *P. trichocarpa* branch	Kahn et al., 2012
WP5	*Rahnella sp.*	Snoqualmie River *P. trichocarpa* branch	Doty et al. 2009
WW5	*Sphingomonas sp.*	Snoqualmie River *Sitka sitchensis* branch	Doty et al. 2009
11R-B1	*Curtobacterium sp.*	Skykomish River *P. trichocarpa* root	This experiment
Yakima River Consortium			
2A	*Microbacterium kitamiense*	*Populus spp.*	Doty, unpublished
2C3	*Rhodococcus erythropolis*	*Populus spp.*	Doty, unpublished
2D1	*Microbacterium kitamiense*	*Populus spp.*	Doty, unpublished
2D2	*Microbacterium kitamiense*	*Populus spp.*	Doty, unpublished
3	*Microbacterium testaceium*	*Populus spp.*	Doty, unpublished
8F	*Microbacterium flavescens*	*Populus spp.*	Doty, unpublished
8L	*Microbacterium hibisci*	*Populus spp.*	Doty, unpublished
8S	*Microbacterium hibisci*	*Populus spp.*	Doty, unpublished
9	*Microbacterium ginsengisoli*	*Populus spp.*	Doty, unpublished
10	*Dyella ginsengisoli*	*Populus spp.*	Doty, unpublished
11	*Microbacterium testaceium*	*Populus spp.*	Doty, unpublished
21Y	*Pseudomonas graminis*	*Populus spp.*	Doty, unpublished
27	*Rhizobium rhizoryzae*	*Populus spp.*	Doty, unpublished
38	*Rhizobium tropici*	*Populus spp.*	Doty, unpublished

2.1 Experiment I

2.1.1 Background and design

Experiment I took place from 05/31/2022 to 08/20/2022. A total of 36 uninoculated *Populus trichocarpa* Nisqually-1 clones were grown aseptically from tissue culture and 18 were inoculated with the DOE endophyte consortium (**Table 2**). Plants were transplanted into separate 8.5-liter pots with an average of 1940 g of sterile rooting media (5-parts peat: 1-part coarse pumice by weight). After transplanting, the pots were placed under a mist tent to promote rooting for one week before moving them to the greenhouse bench where they stayed for 50 days prior to starting the experimental water-deficit. Pots were arranged in a randomized complete block design (RCBD) to isolate plant heterogeneity when applying the abiotic treatments. Blocks were perpendicular to the length of the 5.5 m bench to account for potential temperature or humidity gradients across the North to South ends of the greenhouse. There were 9 blocks in total with one replicate from each treatment group within a block. During the experiment, the plants experienced an average 21.9 **(**±0.4) ^{o}C temperature, 69.6 % (±0.4) % relative humidity, and a 14/10-hour light/dark photoperiod from supplemental LED lamps (ZELION HL300 Grow White, OSRAM Sylvania Inc., Wilmington, MA, USA). Plants were fertigated with a 200 ppm 17-5-17 Nutriculture liquid nutrient solution (Plant Marvel Laboratories Inc., Chicago Heights, IL, USA) in lieu of tap water to maintain nutrition every 2-3 days. Pots were placed in plastic buckets to minimize cross-contamination of endophyte treatments through fertigation run-off.

Calibrating the experimental water-deficit involved creating a simple linear model to estimate different soil-moisture levels of the potting media at an assumed 100% and 0% pot water holding capacity (WHC). Generating this curve consisted of weighing ten additional 8.5-

liter pots with the same type and mass of experimental media under water-saturated and oven-dried conditions (**A1**). Saturation occurred from evenly wetting the media within and across pots and promptly covering the tops to minimize water loss from evaporation. All potted media reached a stable mass after two days, and their values were recorded as 100% WHC. Drying ensued by moving the same pots into a forced air oven at 70 °C. After weighing biweekly for 12 days, all pots reached a consistent mass, and their values were logged as 0% WHC.

Fertigation was reduced randomly for 9 inoculated and 9 control plants 98 days after inoculation and 50 days after the plants were placed on the bench. The soil-moisture deficit was defined from the calibration curve as 35% of the pot water holding capacity (WHC), and the remaining 18 plants received a well-watered treatment (80% of the WHC). Plants in the water deficit group received fertigation at an increased frequency, attempting to account for potential differences in nutrient availability. Pots were weighed every 2-3 days and their mass was converted to WHC using the calibration curve. Plant mass was assumed negligible in the calculation**.** When the mass of a pot fell below its lower target threshold, it was fertigated back to an upper limit weight, such that the WHC could oscillate around the target value (**Fig 1).** Sensors were installed at a consistent depth in each pot to examine the soil moisture tension (200SS Watermark**,** Irrometer Company Inc, Riverside, California). The resulting matric potentials were used to visually assess if the relative water availability for plant uptake differed between the assigned WHC treatment groups.

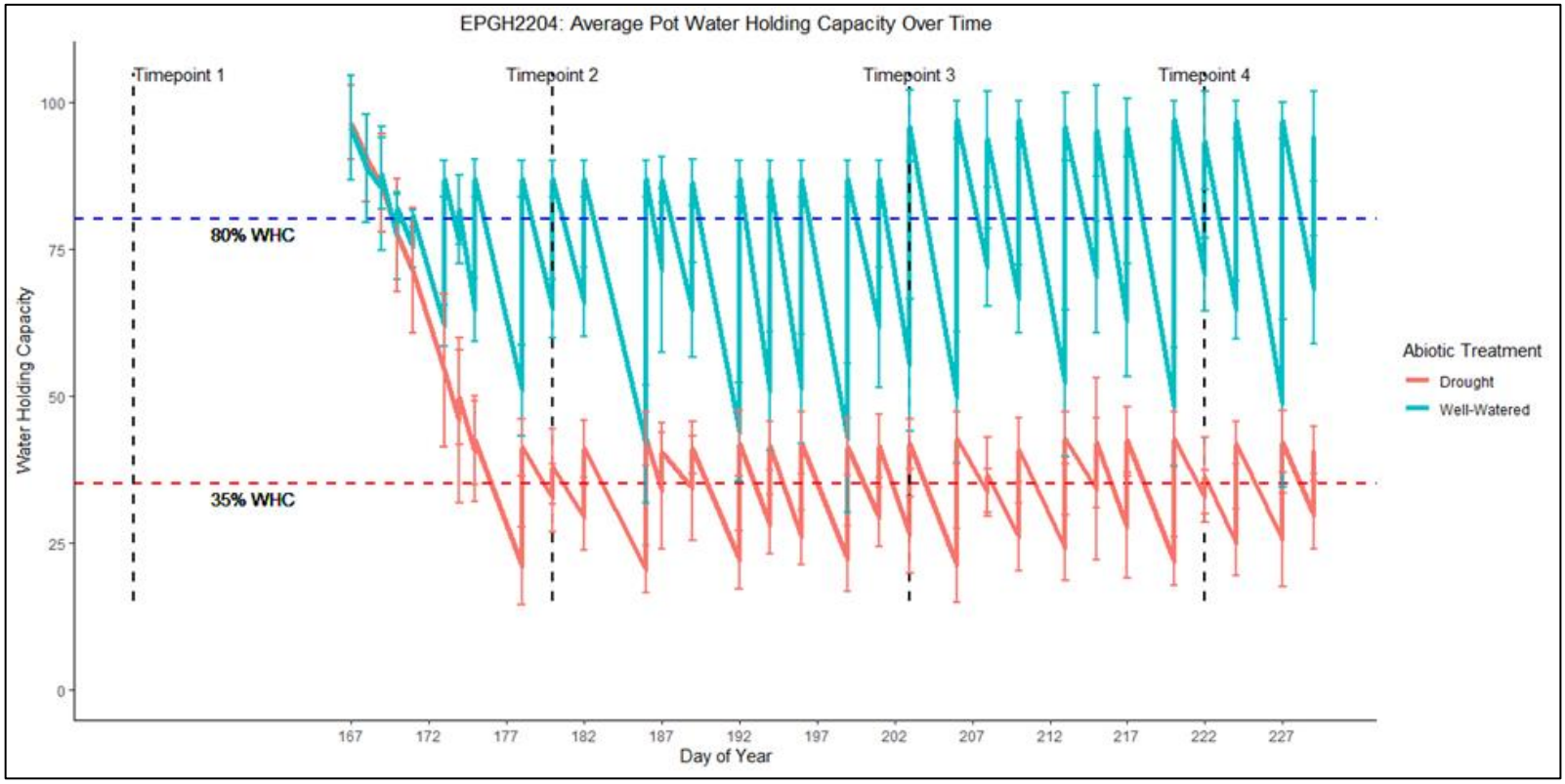

Figure 1. Experiment I: Well-watered (80% WHC) and water-deficit (35% WHC) treatment progression expressed as a percentage of pot water holding capacity (WHC) over time. The blue line indicates the well-watered group, and the red line shows the water-deficit group (drought). Individual pots were weighed every two days and rewatered with nutrient solution to their target WHC based on from an initial calibration curve. Vertical lines represent the sampling timepoints that leaf-exchange and leaf epidermal impressions were taken.

2.1.2 Leaf-gas exchange

Leaf-gas exchange measurements were performed on random subsets of blocks at four sampling timepoints with an open-flow, portable photosynthesis system (LI-COR 6400XT; LI-COR, Lincoln, NE, USA), equipped with a 2 cm^2 chamber head. One sampling timepoint took place before imposing the experimental water stress (t1), and the remaining happened after the water-deficit (t2, t3, t4; **Fig 1**). For each sampled plant, the chamber was clamped to the

youngest, fully expanded, sun-exposed leaf in the middle of the lamina away from the midvein (i.e., 4 – 5 leaves distal to the apical meristem). Before this, each leaf was dark-adapted by wrapping its surface in tinfoil for at least 20 minutes. Within the cuvette, blue and red light was provided with the 6 cm^2 LED source (LI-6400-02B) to generate uniform intensity across the examined leaf area. Using a built-in program of the LI6400, photosynthetic light response curves (*AQ* curves) were generated by increasing the photosynthetic photon flux density (PPFD) discretely from 0 $\mu mol_{photon}\, m^{-2}\, s^{-1}$ to 2000· $\mu mol_{photon}\, m^{-2}\, s^{-1}$ while keeping the reference CO_2 (C_a) at 400 μmol m^{-2}. Measurements were made at 0, 20, 50, 100, 200, 400, 600, 800, 1000, 1500, 2000 $\mu mol_{photon}\, m^{-2}\, s^{-1}$. At each step, net assimilation (A_{net}) was allowed to stabilize to the new chamber condition based on the criteria from the auto program (for 15 seconds, ΔCO2S < 1; ΔH2OS <1; Flow < 1) before logging the output. Constant chamber settings represented ambient environmental conditions on a warm day (leaf temperature, 25°C; Relative humidity, 40-60%; flow rate, 500 μmol s^{-1}). One additional log was made after completing the preset program under the same settings and used as a spot measurement. Diurnal influences were minimized by completing measurements between 8:00-16:00 on the same day.

2.1.3 Stomatal morphology

Leaf impressions were made with dental putty (Colténe/Whaledent AG, Alstätten, Switzerland) from both the top (adaxial) and bottom (abaxial) sides of each plant's youngest, fully expanded, sun-exposed leaf (**A3**). Sampling timepoints matched with leaf gas-exchange (**Fig 1**). Putty was dispensed through a mixing tip to combine the catalyst and base of the solution while applying it evenly over the middle of the lamina and away from the midvein. The same area of the leaf that received gas-exchange was used when applicable. Putty was allowed to dry into a silicone impression before removing it from the leaf. In total, 252 leaf impressions

were taken over the course of the experiment (36 impressions from 18 plants prior to water stress and 72 impressions from all 36 plants for each successive sampling timepoint post water-deficit).

Clear nail varnish was applied on the silicone leaf impressions and allowed to dry before removing the hardened polish with clear adhesive tape (i.e., the positive impression). After mounting the resulting positive impression onto microscope slides, images were taken of each under a microscope (E200 Eclipse, Nikon Instruments Inc., Melville, New York) with a camera attachment (MU-1803 HS, AMScope, Irvine, California) using a constant image resolution (1782x1372 pixels). Image dimensions were converted to a distance by using a calibration ratio created by measuring a stage micrometer with the same image resolution in ImageJ (Schneider et al., 2012). At least three images per impression at every time point were taken under 400x magnification (i.e., 0.068 mm^2/image) to measure individual stoma. Four images per impression were taken at every time point under 100x magnification to determine stomatal density (i.e., 1.104 mm^2/image).

From the images taken at 400x magnification, guard cell length (GCL; µm) and pore length (PL; µm) of 10 stomata were measured across the images for each replicate using ImageJ (Schneider et al., 2012). Following this manual approach, a convolutional neural network (CNN) was further trained and validated (Epochs = 150; IOU = 0.8; Loss = 0.03) with StomataGSmax (Gibbs et al., 2021) by annotating 122 additional photos with a Pixel Annotation Tool (Bréhéret, 2017). Model accuracy was further assessed by relating the manual measurements to those predicted by the model, showing consistent underpredictions (**A2**). Pore width (PW) was determined from StomataGSmax. Stomatal index (SI), or the normalized metric of stomatal density to account for cell expansion, was measured manually by counting cells with the Cell Counter plugin in ImageJ and assisted by cell segmentation from a CNN model developed using

RootPainter (Smith et al. 2022). Each 100x image was first processed by StomataCounter (Fetter et al., 2019), before manual annotation to determine stomatal density (SD; mm^{-2}). Measurements were averaged at the plant level to avoid pseudoreplication. An overview of this process is in the appendix (**A4**). Anatomical maximum stomatal conductance (g_{smax}; mol m^{-2} s^{-1}) was calculated using the size and density data with the equations of Franks & Farquhar (2001) and geometric assumptions were made based on Franks & Beerling (2009) and Wall et al. (2022):

$$Anatomical\ g_{smax} = \frac{SD\ \cdot\ A_p\ \cdot \frac{D}{V}}{d_p + \frac{\pi}{4} + \sqrt{\frac{A_p}{\pi}}}$$

where *SD* is the average stomatal density, *D* is the diffusivity of water in air (2.82×10^{-5} m^2 s^{-1} at 25°C) and *V* is the molar volume of air (m^3 mol^{-1}, at 25°C and 101.3 kPa). Pore depth (d_p; m) was equal to average guard cell width, represented as a quarter of the guard cell length (d_p = GCL/4). The mean maximum stomatal pore area (A_p, m^2) was calculated assuming stomatal pores were circular at maximum opening (Franks & Beerling, 2009), with the diameter equal to pore length ($A_p = (PL/2)^2$).

2.1.4 Data analysis

2.1.4.1 Leaf-gas exchange

Photosynthetic light response curves were created for Experiment I to determine endophyte effects on light saturated assimilation (A_{max}). The three-parameter rectangular hyperbola equation was fitted with non-linear least squares for each treatment at every timepoint (Archontoulis et al., 2015)**:**

$$A_{net} = \frac{\alpha I A_{max}}{\alpha I\ +\ A_{max}} - R_d$$

where A_{net} is the measured rate of net carbon assimilation; α is the apparent photochemical efficiency; I represents the photosynthetic photon flux density (PPFD) absorbed by the leaf; A_{max} is light saturated assimilation; and R_d is the leaf mitochondrial respiration rate (**Table 1**). Quantiles of case resampled bootstraps were used to generate confidence bands and intervals for each curve and parameter, respectively**.** This process involved refitting the curve 1000 times and determining the range of these resampled replicates between the 2.5 and 97.5 percentiles.

Additionally, A_{max} was solved independently by assigning R_d the steady-state value of A_{net} under 0 $\mu mol_{photon}\, m^{-2}\, s^{-1}$. The purpose of this method was to assess its influence on parameter precision. To examine the total amount of energy captured by the plant, gross maximum assimilation (A_{gross}) was calculated as the R_d plus A_{net}.

Each spot measurement underwent univariate hypothesis testing to determine treatment differences. Non-parametric permutational ANOVA tests were used to avoid making data assumptions about normality, equal variance, or sphericity (Frossard & Renaud, 2021). These were chosen in favor of parametric tests due to less restrictions, and the ability to yield nearly identical significance levels when model structures are the same. For the pre water-stress observation (t1), mixed effect models were used to compare each trait between inoculated and control plants. Blocking terms were modeled as random effects to reduce unexplained variability. Post water deficit observations also used mixed effects models to compare fixed effects of endophyte treatments, water-stress, timepoint, and two-way interaction terms, assuming a codependent influence on gas-exchange. Plants were considered as the random variable to capture the within sample correlation from repeated measures. Post-hoc contrast analyses within time were examined using Wilcoxon-Mann-Whitney tests for pairwise comparisons. Statistical

significance was determined if values were lower than the type I error rate ($\alpha = 0.05$). Corrections were not used to control the false discovery rate for the multiple *a priori* tests but were used *a posteriori* via the Bonferroni-Holm corrections. Adjusted Partial eta squared ($adj\ \eta_p^2$) effect sizes were generated for each result (**A9** and **Table 5**) as follows:

$$adj\ \eta_p^2 = \eta_p^2 - (1 - \eta_p^2)\frac{df_{effect}}{df_{error}}$$

This estimand was chosen to minimize the bias associated with increasing sample size and avoid possible overestimations of the effect on the population (Mordkoff 2019).

2.1.4.2 Principal component analysis of stomatal morphology

Traits of stomata morphology could be blended into new variables through principal component analysis (PCA) because they were highly correlated (**A15**). Virtually, this reduced the 13 stomatal traits into two composite variables, or principal components (PCs) that represented trends in stomatal patterning. Interpretations of PCs were based on the magnitude and sign of each vector associated with an individual stomatal trait. In other words, traits with similar weights were combined into a PC. The purpose of this analysis was to examine the changes in stomatal patterning from the treatments. Though all PCs were initally examined, only the first two were chosen to simplify the interpretation. PCA biplots were generated to illustrate the trends of PC1 and PC2 in relation to inoculation and the water-deficit. Treatment differences between principal components were interpreted as significant trends in stomatal patterning. The statistical model had the same structure as described for spot measurements. This was used as an alternative to performing several hypothesis tests to compare each individual stomatal trait among treatments. However, results from these hypothesis tests can be found in the appendix (**A6-9**).

2.1.4.3 Stomatal patterning

A multivariate permutational analysis of variance (PERMANOVA) was used to compare the treatment effect on stomatal patterning (Anderson 2001). This assumed the accumulated difference from individual stomatal traits could reveal a collective difference (**Table 1**). Statistically, this test was used to avoid making underlying assumptions about multivariate normality or homogeneity of variance, while minimizing the false discovery rate from using several univariate hypothesis tests (Anderson 2017). PERMANOVAs were used separately for each sampling timepoint to examine variation of stomatal patterning within the water deficit progression. Exploratory analysis showed that time and inoculation did not interactively affect individual stomatal traits (**A6**); therefore, all post water stress observations were aggregated to examine the average treatment effects on stomatal patterning. Sequential sum of squares (i.e., type I or terms) was used to allow treatment factors placed first in the model explain most of the variation**.** Prior to the statistical tests, each stomatal trait was rescaled as a proportion of its range (i.e., min-max normalized). Effectively, this preserved the observed relationships within each stomatal trait but gave equal importance across traits. The similarity of stomatal patterning between each plant was determined by generating a Euclidean distance matrix.

2.1.4.4 Corresponding stomatal patterning with conductance

For experiment I, principal component regression (PCR) was used to correspond stomatal patterning with conductance in part to avoid multicollinearity from using individual traits of stomatal anatomy as dependent variables. All post water stress observations were aggregated to simplify the analysis under the justification that the correlation structure of stomata patterning was well preserved over time (**A15**). Initially, predictors of the linear model included the two

PCs, inoculation, and water-stress treatments, and blocking terms. Operational g_{sw} under light saturation (2000 $\mu mol_{photons}\ m^{-2}\ s^{-1}$) was the response. Global models were then reduced using domain knowledge by removing the most complex terms, often the interactions. The final model was selected to balance complexity with parsimony and consisted of each PC and the blocking term. This method assumed that inoculation status was reflected through the principal components. Mixed effects models were again used, considering the blocking term as a random effect and the PCs as fixed. Conditional R^2 was chosen to evaluate the model, which allowed both the PCs and blocking effects explain the response in stomatal conductance. Maximum likelihood was used to estimate the parameters, which allowed for significance testing of models.

2.2 Experiment II

2.2.1 Background and design

Experiment II took place from 08/19/2022 to 11/15/2022. A total of 76 uninoculated *Populus trichocarpa* Nisqually-1 ramets were grown aseptically from tissue culture. From the total, 26 of the trees were inoculated with the 8-strain DOE mix; another 24 were inoculated with the 14-strain Yakima River mix; and the remainder were left uninoculated (**Table 2**). Most protocols of this study followed those from experiment I with few exceptions. Plants were propagated into separate 8.5 L pots with an average of 1800 g of sterile rooting media (Sunshine Mix #2, Sun Gro Horticulture). After transplanting, pots remained under the mist tent for two weeks before moving to the greenhouse benches where they stayed for 30 days prior to starting the experimental water-deficit. Fertigation used a solution of 17-17-17 NPK at 250 ppm and took place every 1-2 days, depending on the pot WHC from a newly developed calibration curve, which was developed following the same method as described in Experiment I.

2.2.2 Stomatal morphology

Sampling and measurements of stomatal morphology followed similar guidelines as experiment I with a few key differences. Measurements happened at three sequential occasions throughout the study. One sampling timepoint took place before imposing water stress (t1) and the remaining happened after beginning the experimental water-deficit (t2, t3; **Fig 2**). In total, 376 leaf impressions were taken over the course of the experiment (72 impressions from 36 plants prior to water stress and 152 impressions from all 76 plants for each successive sampling timepoint post water-deficit).

Microscopy procedures were similar for this experiment except that 10 images per impression at every time point were taken under 400x magnification (i.e., 0.068 mm^2/image) to measure individual stoma. From the images taken at 400x magnification, the CNN model trained and validated with StomataGSmax (Gibbs et al., 2021) was used to measure stoma dimensions. Stomatal index (SI) was not examined due to time constraints, and all other measurements were conducted the same as Experiment I.

2.2.3 Data analysis

2.2.3.1 Stomatal traits

Analyzing the stomatal morphology data from this experiment followed the same protocol as described in experiment I. However, this experiment had 13 blocks and the inoculation factor now included three levels: CTRL, DOE, YR (**Table 3**).

2.2.4 Statistical and graphing software

All analysis was performed in R v4.2.2 (R Core Team, 2023), using *tidyverse* functions (Wickham et al., 2019). PERMANOVA was run with the *adonis2* function from v*egan v2.6-4;* univariate parametric and permutational ANOVAs were performed with the *aovperm* function from *permuco v1.1.2*; PCA biplots were created using *ggbiplot v0.55;* correlograms were generated with the *ggcorrplot v0.1.4* package; model selection and exploration was done with *MuMIn v1.47.1, lmerTest v3.1-3, and lme4 v1.1-33;* confidence intervals and bootstraps were generated with *boot v1.3-28*; non linear least squares fitting was performed using *nls.multstart v1.2.0*; violin plots and response curves were created using *cowplot v1.1.1* and *ggh4x v0.2.4*. Inkscape *v1.2.0*, a vector-based imaging editor, was used to increase text size after exporting figures from R.

Figure 2. Experiment II: Well-watered (80% WHC) and water-deficit (35% WHC) treatment progression expressed as a percentage of pot water holding capacity (WHC) over time. The blue line indicates the well-watered group, and the red line distinguishes the water-deficit group. Individual pots were weighed every two days and rewatered with nutrient solution to their target WHC based on from an initial calibration curve. Vertical lines represent the three sampling timepoints.

Table 3. Summary tables of the two greenhouse experiments presented in this paper, highlighting the key differences between both. Average values of environmental data given (± SD).

*Average daily light integral (DLI; $mol_{photon}\ m^{-2}\ day^{-1}$) represents daily solar irradiance values (MJ m-2 day-1) obtained from a weather station located outside the greenhouse (AgWeatherNet, WSU, 2023). Note the true DLI values plants experienced are different from these values because of the transmission through glazing materials, obstruction by greenhouse structure, and supplemental lighting.

	Experiment 1	Experiment 2
Water-deficit length	Summer (06/15/2022 - 08/17/2022); 64 days	Summer through Fall (08/19/2022 - 11/15/2022); 91 days
Inoculation date	03/09/2022	06/08/2022
Endophyte consortia	DOE	DOE and YR
Experimental design	Randomized complete block design; 2x2 factorial	Randomized complete block design; 2x3 factorial
Fertigation regime	17-5-17 NPK at 200 ppm; supplied every 2-3 days depending on pot WHC	17-17-17 NPK at 250 ppm every 1-2 days depending on pot WHC
Average daily light integral*	47.1 mol m^{-2} day^{-1} (± 14.4)	24.9 mol m^{-2} day^{-1} (± 12.6)
Average Relative humidity	69.6 % (± 8.75)	66.4 % (± 12.3)
Average temperature	21.9 ^{o}C (± 1.3)	20.8 ^{o}C (± 1.93)
Powdery mildew observed	No	Yes

3 Results

3.1 Experiment I

3.1.1 Leaf-gas exchange

3.1.1.1 Light response curves

Modeled gas-exchange parameters were examined from the light response curves (**Fig 3).** Inoculation marginally impacted the maximum assimilation rate (A_{max}) prior to water stress (p = 0.056; $adj\ \eta_p^2$ = 0.16), showing lower values relative to the control. No other changes were observed in underlying biochemical parameters **(Fig 4)**.

After initiating water stress, inoculation had no effect on any of the biochemical parameters. Mitochondrial respiration (R_d) decreased over time (p = 0.006; $adj\ \eta_p^2$ = 0.19) but did not experience any treatment effects. The water-deficit reduced A_{gross} (p<0.001). Water stress compounded with time to decrease A_{max} (p < 0.007; $adj\ \eta_p^2$ = 0.18) but showed a fluctuating effect on the apparent photochemical efficiency (α), decreasing it at the third observation before resurging at the final sampling timepoint (p = 0.037; $adj\ \eta_p^2$ = 0.11; **Fig 4**).

Estimating R_d and then refitting the curve did not visually alter the curve or lead to different conclusions.

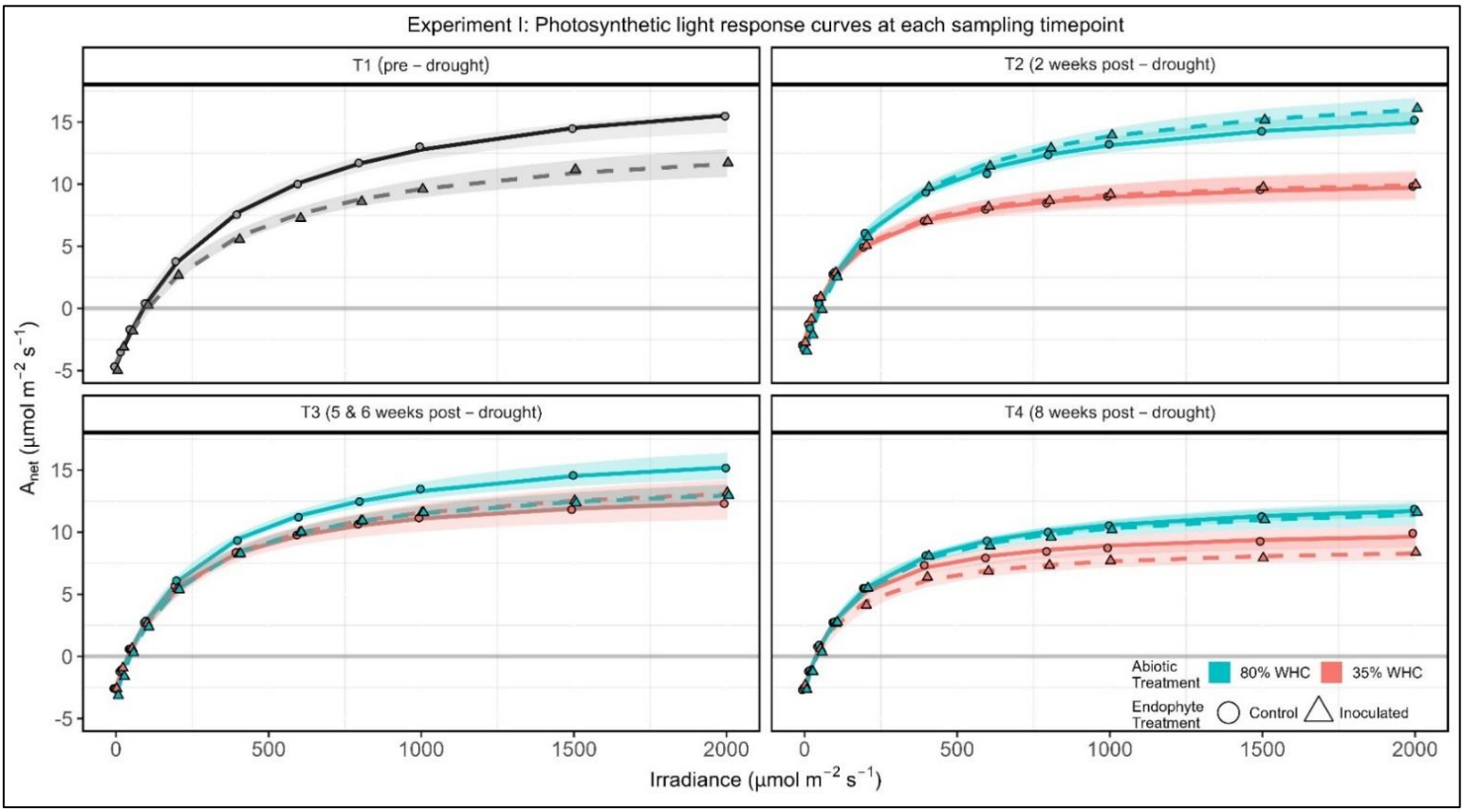

Figure 3. Photosynthetic light response curves (AQ) from uninoculated (control; circles) and endophyte-inoculated (triangles) *Populus trichocarpa* before (grey-shaded) and after experiencing well-watered (blue; 85% of the pot water holding capacity) and water deficit (red; 35% of the pot water holding capacity) conditions. Curves were generated from fitting the three-parameter rectangular hyperbola equation (RH) to each treatment group with non-linear least squares. Points represent mean values. Confidence bands were created from the quantiles of case-resampled bootstrap replicates (n = 1000).

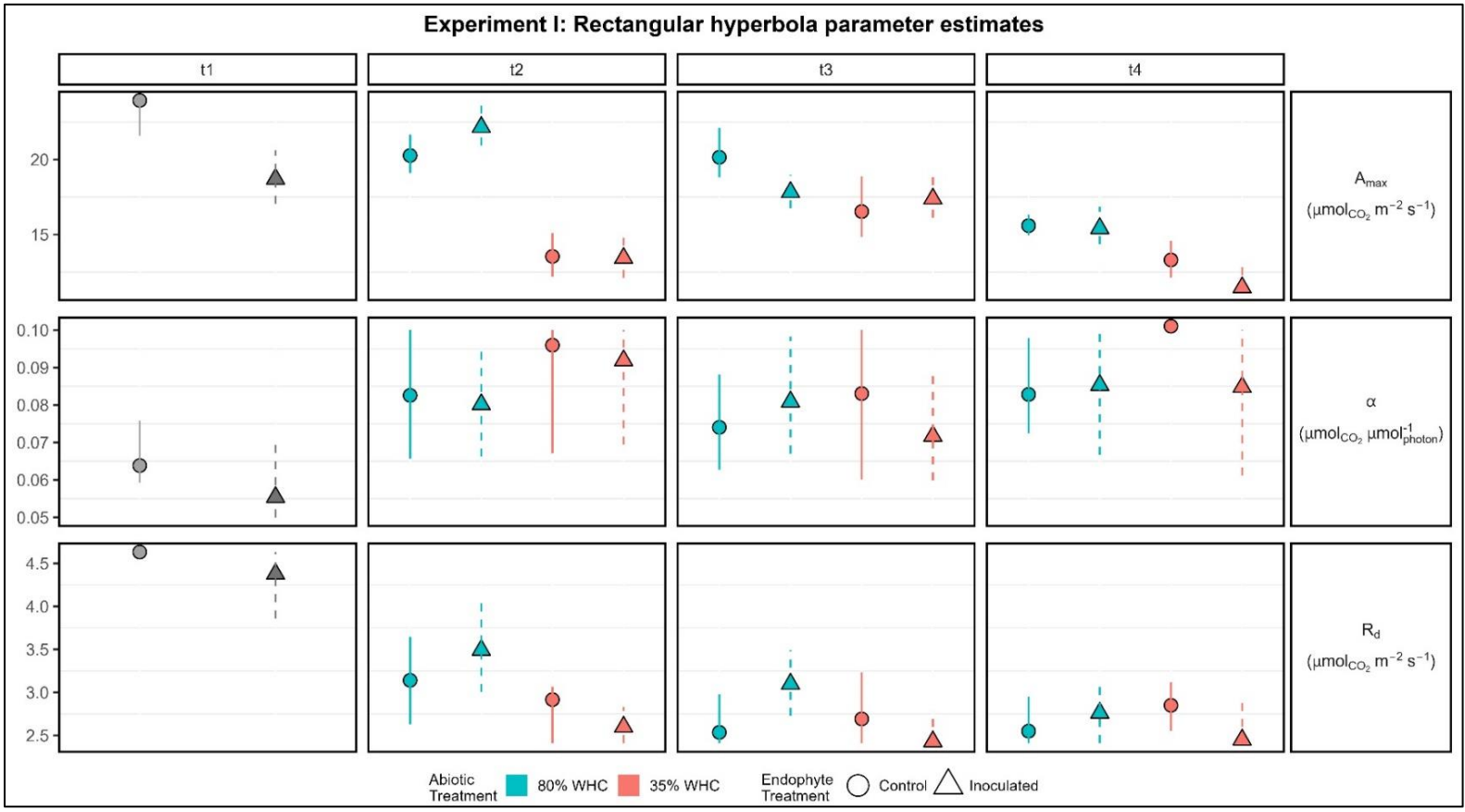

Figure 4. Dot plots of modeled parameter estimates from the fitted rectangular hyperbola equation to the response of carbon assimilation against stepwise changes in irradiance. Associated statistics are listed in section 3.1.1.1 Light Response Curves. Measurements were taken from the youngest, fully expanded leaf of uninoculated (control; circles) and endophyte-inoculated (triangles) *Populus trichocarpa* pre (shaded) and post water-deficit. Blue represents well-watered (80% WHC) and red illustrates water-deficit (35%) soil-moisture conditions. Enlarged shapes represent the mean and lines illustrate the 95% confidence intervals of the net assimilation rate (A_{max}), apparent photochemical efficiency (α), and mitochondrial respiration (R_d). Confidence intervals were created from the quantiles of case-resampled bootstrap replicates (n = 1000). Statistics are referenced within the text.

3.1.1.2 Spot gas-exchange measurements

Spot measurements of leaf gas-exchange were examined for all treatments. Prior to water stress (t1), endophyte inoculation from the DOE mix significantly reduced the net carbon assimilation rate (A_{net}) and intrinsic water-use efficiency (*iWUE*) under light saturation (2000 $\mu mol_{photons}\, m^{-2}\, s^{-1}$; (**Table 4; Fig 5**). However, inoculation showed no effect on stomatal conductance (g_{sw}; p = 0.44). Control plants had larger A_{net} values, leading to higher *iWUE* (**Fig 5**). Similarly, inoculation only marginally impacted leaf transpiration (*E*), which lead to a reduced extrinsic water-use efficiency (*WUE*; **Table 4**; **A5**).

After the water-deficit treatment started, inoculation showed no changes in A_{net} while lowering g_{sw}, increasing *iWUE*. This effect was independent of both time and soil-moisture status; therefore, only the main effects are illustrated (**Table 4; Fig 5**). Leaf transpiration dropped over time (p <0.001), with water-stress (p <0.001), and marginally from inoculation (p<0.077; **A5**). The water-deficit tended to increase *iWUE*, and over time, it decreased A_{net} and g_{sw} (**Table 4; A5**)**.** *WUE* followed similar trends as *iWUE*, showing increases from inoculation (p = 0.04) as well as water-stress (p = 0.001) and time (p = 0.002). Notably at the final sampling timepoint, inoculated plants experiencing the water-deficit showed the largest increase in *iWUE* (Cohen's d = 1.03; p = 0.068) and *WUE* (Cohen's d = 0.85; p = 0.121) relative to the control with the same soil-moisture status (**A5**).

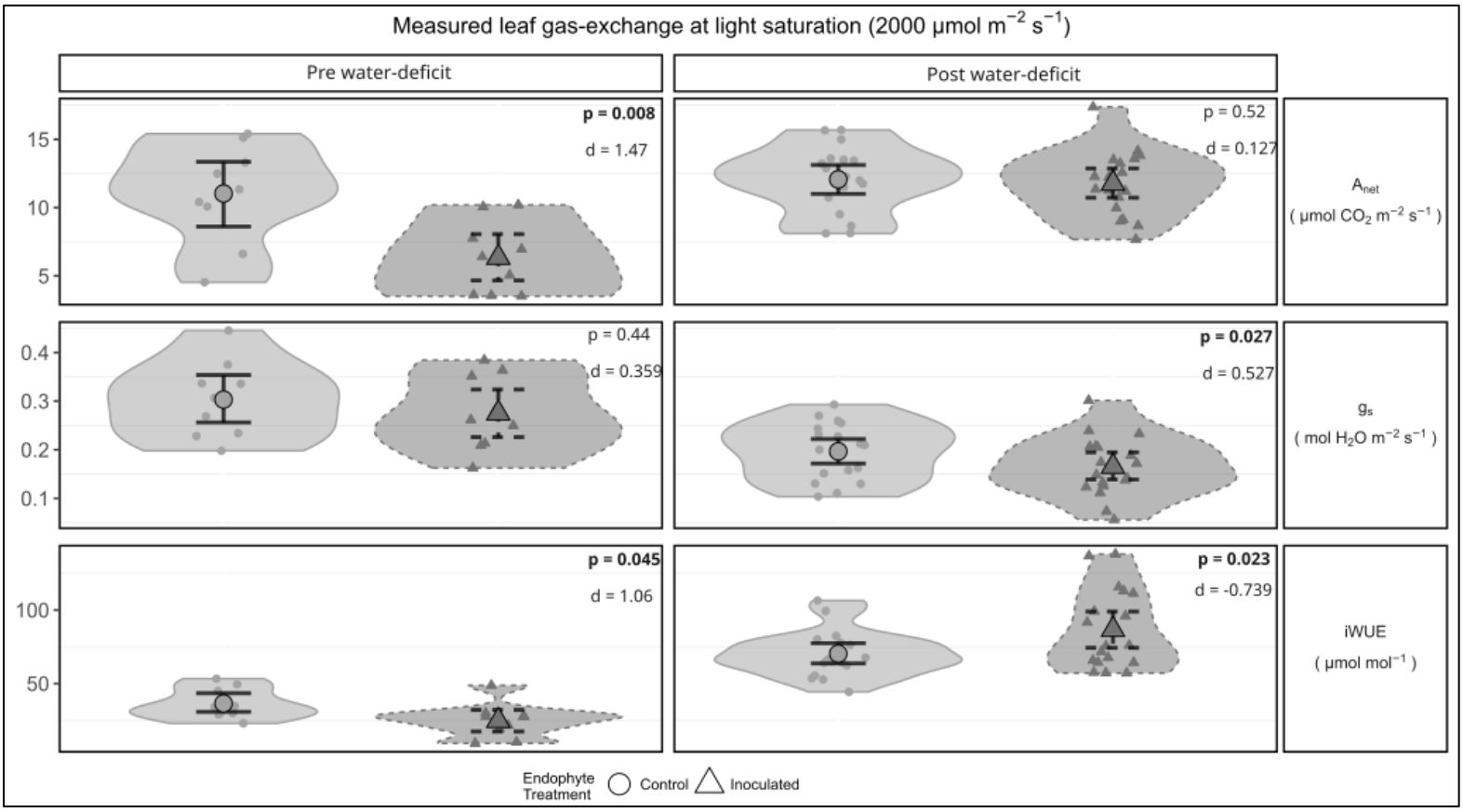

Figure 5. Experiment I: main effect plots of leaf-gas exchange taken at light saturation (2000 µmol photons m^{-2} s^{-1}) from the youngest, fully expanded leaf of uninoculated (control; circles) and endophyte-inoculated (triangles) *Populus trichocarpa* pre and post water-deficit. This includes plants from both 80% and 35% WHC groups. Enlarged shapes represent the mean and lines illustrate the 95% confidence intervals of the net assimilation rate (A_{net}), stomatal conductance (g_{sw}), and intrinsic water-use efficiency (*iWUE*). Cohen's d effect sizes shown for comparisons of inoculation treatments to express the magnitude of mean differences. Confidence intervals were created from the quantiles of case-resampled bootstrap replicates (n = 1000).

3.1.2 Principal component analysis of stomatal morphology

Most of the leaf stomatal traits from this experiment were highly correlated and maintained this pattern regardless of sampling timepoint (**A15**; **Fig 6**-**Fig 7**). Therefore, these individual traits could be blended into composite principal components to reveal trends of stomatal patterning. Generally, stomatal size traits inversely correlated with density, and both

were orthogonal to stomatal ratio and index. However, there were a few exceptions in this data that deviated from this generalization: the correlation between adaxial stomatal density and size traits seemed to disappear at sampling timepoint 3 and slightly resurged at timepoint 4. Another observation was that the strength of the relationship between anatomical g_{smax} and stomatal size diminishes post water-deficit.

At each timepoint, the first two principal components (PCs) accounted for more than 58% of the variation (**A16**; **A17**). While interpretation of the principal components was subjective, it was based on the weight of each stomatal trait and its relative direction to one another (**A16**). In other words, traits within a PC that had the same weight could be blended into a composite variable. Before the water-deficit, PC1 gave roughly equal weight to all variables except stomatal ratio. Traits that represented stomatal dimensions had opposite signs of those associated with numbers. This was interpreted as the tradeoff between stomatal size and density and accounted for 49.1% of the variance in the stomatal variables. PC2 gave most weight to stomatal ratio and adaxial density, index, and anatomical g_{smax}, and was interpreted as the distribution of stomata to leaf side, driven by shifts in adaxial stomatal numbers. This accounted for 16.0% of the variation. Along PC1, increasing values represented plants with larger, more sparse stomata, whereas decreasing values depicted plants with denser, smaller stomata. For PC2, decreasing values portrayed plants with higher stomatal ratios due to more adaxial stomata.

Although the loadings changed post water-stress, the interpretation of the PCs shared the same understanding as those pre-water-stress (**A16**). PC1 gave similar weights to all stomatal size traits and bottom stomatal density. This accounted for 47.2% of variation in the response variables and was interpreted as the tradeoff between stomatal size and abaxial density. PC2 gave similar weight to stomatal ratio, but also to adaxial density, index, and anatomical g_{smax}.

This accounted for 19.4% of the variation and was again determined as stomatal ratio, influenced by increases in adaxial stomatal numbers. Along PC1, increasing values represented plants with larger stomata and less density on the abaxial leaf surface; decreasing values portray plants with smaller stomata, with more on the abaxial surface. For PC2, increasing values depicted plants with higher adaxial stomatal ratios due to more adaxial numbers; decreasing values showed plants with lower ratios from less adaxial stomata (**Fig 6-7**).

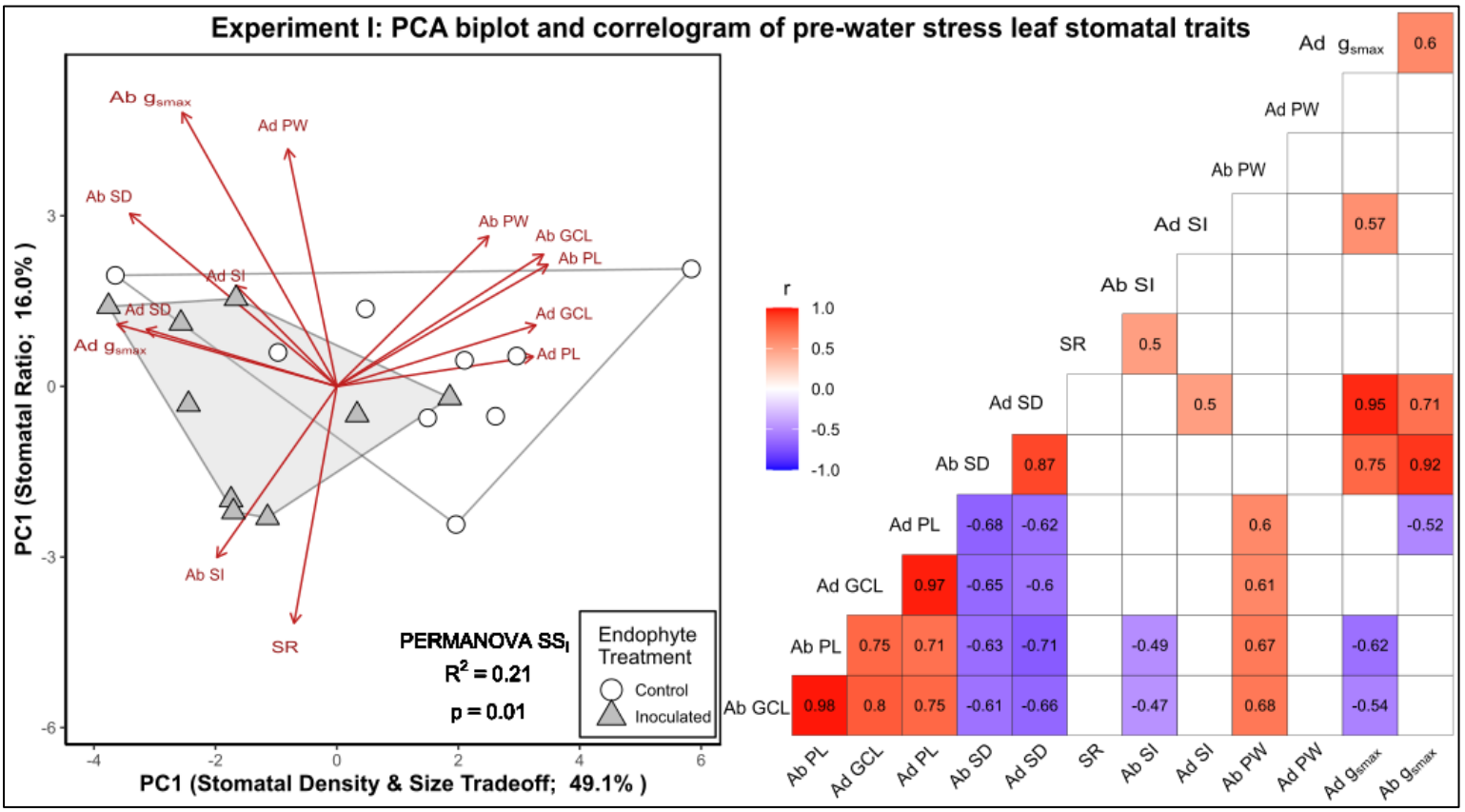

Figure 6. Two-dimensional Principal Component Analysis (PCA) biplot (left) and correlation matrix (right) of stomatal patterning traits from pre-water-deficit *Populus trichocarpa*. Based on magnitude and direction of vectors, PC1 represents the tradeoff between stomatal density and size; PC2 shows the distribution of stomata to leaf sides. Pearson's correlation coefficient (r) is shown for each significant relationship ($p < 0.05$) along with either red or blue colors indicating positive or negative correspondence, respectively. Blank cells represent nonsignificant correlations. For both adaxial (Ad) and abaxial (Ab) leaf surfaces, examined traits include guard cell length (GCL), pore length (PL), pore width (PW), stomatal index (SI), anatomical maximum stomatal conductance (g_{smax}), stomatal density (SD), and stomatal density ratio (SR).

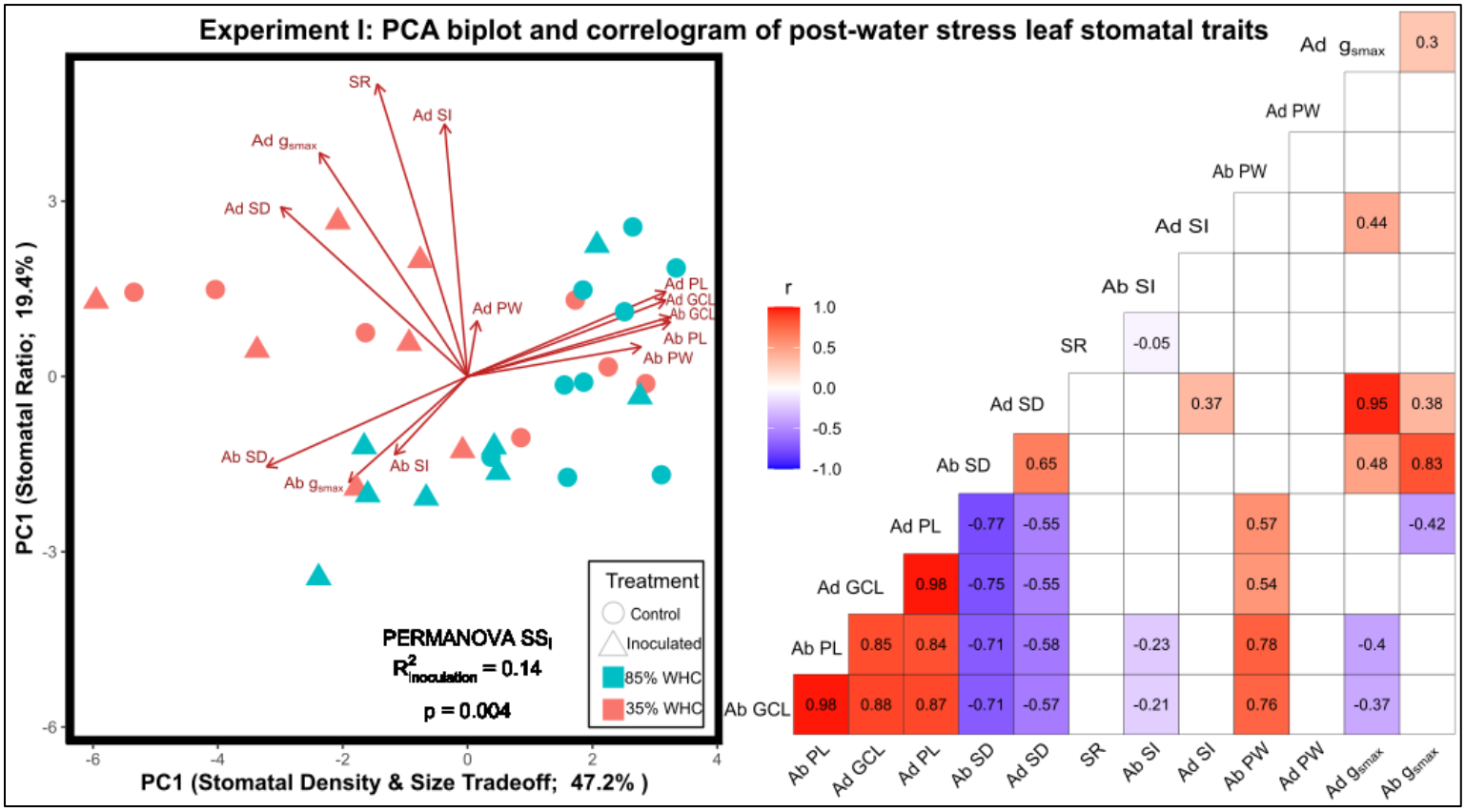

Figure 7. Two-dimensional Principal Component Analysis (PCA) biplot (left) and correlation matrix (right) of stomatal patterning traits aggregated from the post water-stress sampling timepoints in *Populus trichocarpa*. Based on magnitude and direction of the vectors, PC1 represents the tradeoff between stomatal density and size; PC2 shows the distribution of stomata to leaf sides, driven by increases in adaxial numbers. Pearson's correlation coefficient (r) is shown for each significant relationship ($p < 0.05$) along with either red or blue colors indicating positive or negative correspondence, respectively. Blank cells represent nonsignificant correlations. For both adaxial (Ad) and abaxial (Ab) leaf surfaces, examined traits include guard cell length (GCL), pore length (PL), pore width (PW), stomatal index (SI), anatomical maximum stomatal conductance (g_{smax}) stomatal density (SD), and stomatal density ratio (SR).

Prior to water stress (t1), endophyte inoculation from the DOE mix significantly altered the stomatal density and size relationship (PC1*;* **Table 4**; **Fig 6**). Inoculated plants tended to have smaller, denser stomata with greater anatomical maximum stomatal conductance (g_{smax}) relative to the control. No effects were seen on the distribution of stomatal numbers to leaf side (PC2). After starting the water-deficit treatment, inoculation continued to affect the stomatal density and size relationship, independently of water-stress and time (**Table 4**; **Fig 7**). Likewise, the water-deficit also significantly impacted this relationship (**Table 4**; **Fig 7**). No time or interactive effects were seen on these generalized trends of stomatal patterning (**Table 4**).

Table 4. Experiment I: effect sizes (adj η_p^2) of each treatment for the examined traits before and after water-stress. Significant terms ($\alpha = 0.05$) are bolded and based on non-parametric ANOVA models (see Methods and Results). Examined traits include PC1, interpreted as the tradeoff between stomatal density and size and PC2, interpreted as the stomatal density ratio driven by shifts in adaxial numbers. Gas exchange parameters from response curves at 2000 $\mu mol_{photon}\ m^{-2}\ s^{-1}$ include net assimilation (A_n; $\mu mol\ m^{-2}\ s^{-1}$); operational stomatal conductance (g_{sw}; $mol\ m^{-2}\ s^{-1}$); intrinsic water-use efficiency (*iWUE*; $\mu mol\ mol^{-1}$); transpiration (*E*; $mol\ m^{-2}\ s^{-1}$); extrinsic water-use efficiency (*WUE*; $\mu mol\ mol^{-1}$); leaf temperature (T_{leaf}; °C). Values labeled with '*' had marginal significance ($p < 0.1$)

	PC1	*PC2*	A_n	g_{sw}	*iWUE*	*E*	*WUE*	T_{leaf}
	Stomatal density and size tradeoff	*Stomatal ratio*						
	Pre-water deficit							
Inoculation	**0.28**	0.01	**0.34**	0	**0.19**	0.02*	**0.16**	0.01
Post-water deficit								
Inoculation	**0.10**	0	0	**0.05**	**0.05**	0.03*	**0.05**	0.00
Water-deficit	**0.12**	0	**0.24**	**0.25**	**0.12**	**0.24**	**0.08**	**0.06**
Inoculation x Water-deficit	0.01	0	0	0	0	0	0	0
Timepoint	0	0	**0.21**	**0.20**	**0.06**	**0.28**	**0.11**	**0.09**
Inoculation x Time	0.001	0	0	0	0.02	0	0.02	0
Water-deficit x Time	0.02	0.02	**0.07**	**0.08**	0.01	**0.09**	0	0

3.1.3 Treatment differences of stomatal patterning

Inoculation impacted the stomatal patterning prior to the experimental water-stress. In addition, aggregating all post water-deficit observations revealed significant endophyte and water stress effects (**A13**). However, the significance and importance of inoculation on stomatal patterning varied with sampling timepoint (**A14**), showing relatively high explanatory power prior to water stress ($R^2 = 0.21$; $p = 0.01$), but notably less at various times in the drought ($0.04 < R^2 < 0.13$).

Similarly, the significance and relative importance of water stress in explaining the variation of leaf stomatal patterning changed when examining individual sampling timepoints Water-deficit effects at timepoints 2 ($R^2 = 0.13$; $p < 0.01$) and 4 ($R^2 = 0.13$; $p < 0.01$). Aggregating all post water-deficit observations showed significant water-deficit effects ($R^2 = 0.13$; $p < 0.01$).

3.1.4 Relating stomatal patterning to conductance

Principle component regression (PCR) was used to determine the relationship between the principal components of stomatal traits with operational g_{sw} under light saturation (2000 $\mu mol_{photons}\, m^{-2}\, s^{-1}$). Before water stress, the model containing both PC1 (stomatal density & size tradeoff) and PC2 (stomatal ratio, driven by increases in adaxial density) marginally related to g_{sw} ($R^2_{conditional} = 0.24.$; $p = 0.1$). After the water-deficit, the model containing PC1 and PC2 corresponded to g_{sw} and had notable explanatory power when allowed to vary with soil moisture status ($R^2_{conditional} = 0.63$; $p = 0.002$). While PC1 was a significant predictor within each water level ($p < 0.001$ for both), PC2 only related to g_{sw} under well-watered conditions ($p =$

0.04). The fitted relationship between g_{sw} and PC1 showed a negative relationship, meaning as operational g_{sw} increased so did the magnitude of the PC scores representing larger, sparser stomata with lower anatomical g_{smax} (**Fig 8**). PC2 also showed this direct relationship, meaning as operational g_{sw} increased so did the magnitude of the PC scores representing higher ratios due to increases in adaxial stomatal numbers (**Fig 8).**

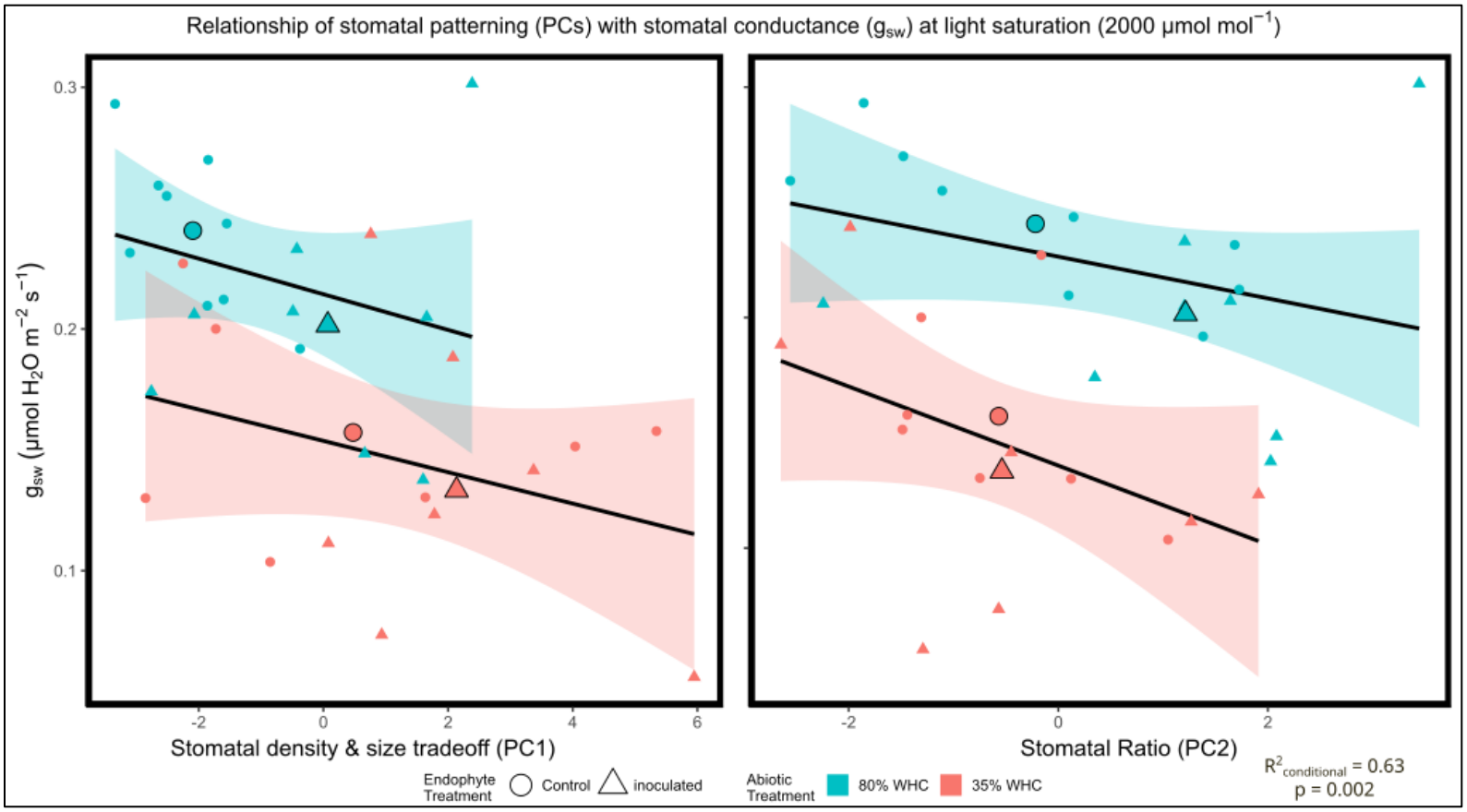

Figure 8. Principal component regression (PCR) illustrating the relationship between stomatal patterning and conductance of uninoculated (circles) and inoculated (triangles) plants under well-watered (80% WHC; blue) and water-deficit (35% WHC; red) conditions. Principal components (PCs) encompass 13 traits relating to stomatal morphology, and operational conductance (g_{sw}) was taken at light saturation (2000 $\mu mol_{photons}\ m^{-2}\ s^{-1}$). PC1 represents the tradeoff between stomatal density and size – positive values indicate smaller and denser stomata with greater anatomical g_{smax}; decreasing values represent larger, sparser stomata with lower anatomical g_{smax}. PC2 depicts shifts in stomatal ratio, driven by changes in adaxial numbers – positive values portray lower ratios due to decreases in adaxial stomata, negative values represent higher ratios from increases in adaxial stomata. Enlarged shapes illustrate the mean value for stomatal patterning and conductance of each treatment (i.e., the group centroid) to assist with interpretation of the trends.

3.2 Experiment II

3.2.1 Stomatal anatomy

In this experiment inoculation showed no significant effects on any stomatal traits before and after the water stress (**Table 5**). Examining pairwise comparisons revealed mostly effects from abiotic stress rather than inoculation with either consortium of endophytes (**Fig 9 – 11; A18**).

Table 5. Experiment II: effect sizes (adj η_p^2) of each treatment for the examined traits before and after water-stress. Significant terms ($\alpha = 0.05$) are bolded and based on parametric ANOVA models or the permutation-based equivalent (see Methods and Results). Significant interaction terms are illustrated in the accompanying violin-plots (see Figures). For both adaxial (Ad) and abaxial (Ab) leaf surfaces, examined traits include guard cell length (GCL; µm), pore length (PL; µm), pore width (PW), maximum anatomical stomatal conductance (g_{smax}; mol m^{-2} s^{-1}), stomatal density (SD; mm^{-2}), and stomatal density ratio (SR). Values labeled with '*' had marginal significance ($p < 0.1$).

	GCL		PL		g_{smax}		SD		PW		SR
	Ad	Ab	Ad	Ab	Ad	Ab	Ad	Ab	Ad	Ab	
Treatment	Pre-water-deficit										
Inoculation	0	0.005	0	0.004	0	0	0.04	0.02	0	0	0
	Post water-deficit										
Endophyte	0	0	0.01	0	0.03*	0	0.02	0	0.04*	0	0.01
Water-deficit	0	0	**0.06**	0	0	0.02*	0.01	0.01	**0.03**	0.01*	**0.05**
Endophyte x Water-deficit	0	0	0	0	0	0	0	0	0	0.02	0
Time	0	**0.55**	**0.15**	**0.24**	**0.29**	0	**0.17**	0.02*	**0.07**	**0.44**	**0.06**
Endophyte x Time	0.01	0	0	0	0	0	0	0	0	0	0
Water-deficit x Time	**0.03**	**0.04**	**0.06**	**0.03**	**0.06**	**0.06**	0.01	**0.03**	0.02*	0.01*	**0.07**

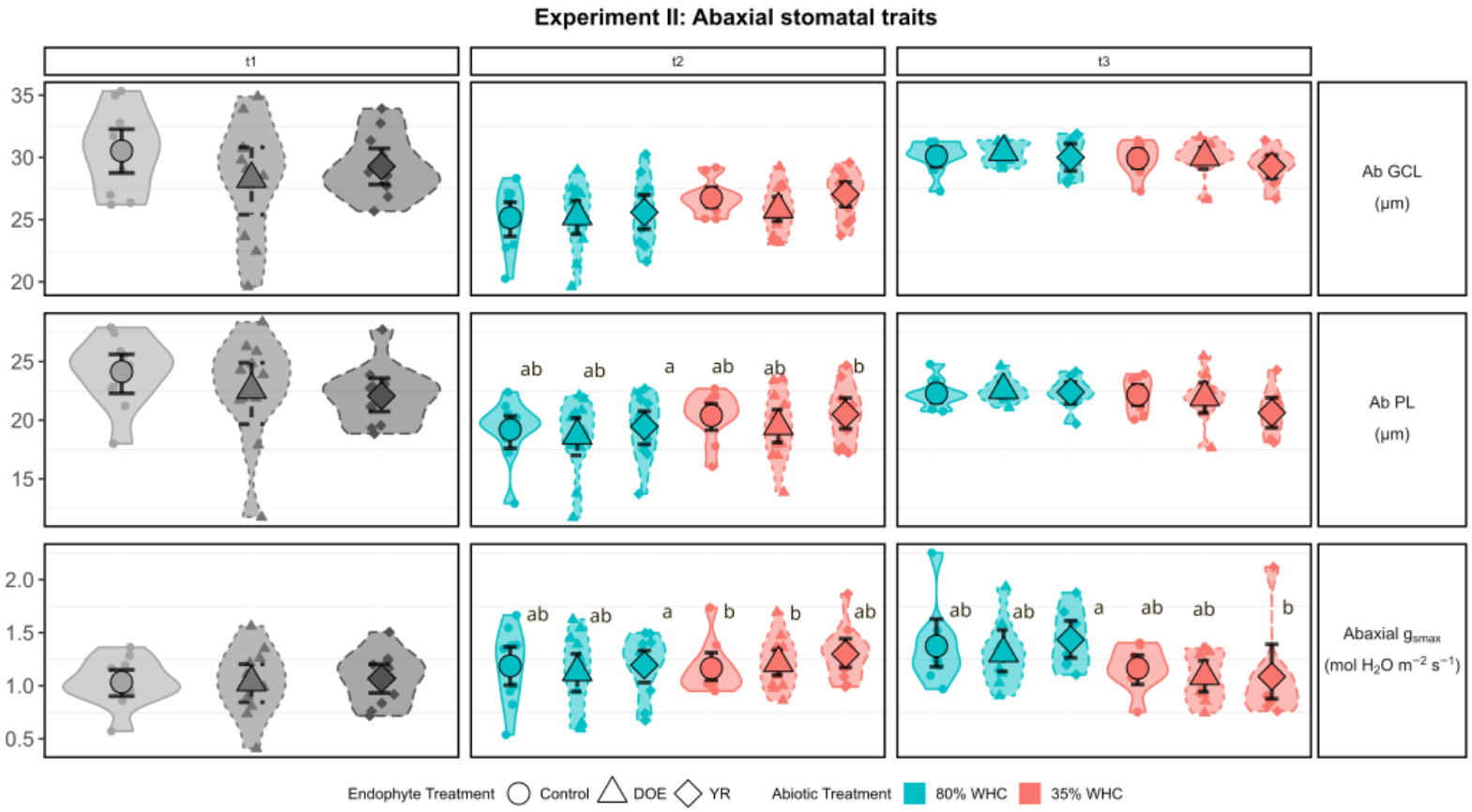

Figure 9. Experiment II: violin plots of abaxial stomatal anatomy from uninoculated (control; circles) and endophyte-inoculated (triangles) *Populus trichocarpa* pre (shaded) and post water-deficit. Blue represents well-watered (80% WHC) and red illustrates water-deficit (35%) soil-moisture conditions. Enlarged shapes represent the mean and lines illustrate the ±95% confidence interval of guard cell length (GCL), pore length (PL), stomatal index (SI), and anatomical maximum stomatal conductance (g_{smax}). Compact letter display (CLD) used to represent significant differences ($P < 0.05$) between treatment means, using the results of Wilcoxon-Mann-Whitney tests for pairwise *post-hoc* tests. Confidence intervals were created from the quantiles of case-resampled bootstrap replicates (n = 1000). Overall effect sizes are given in Table 5.

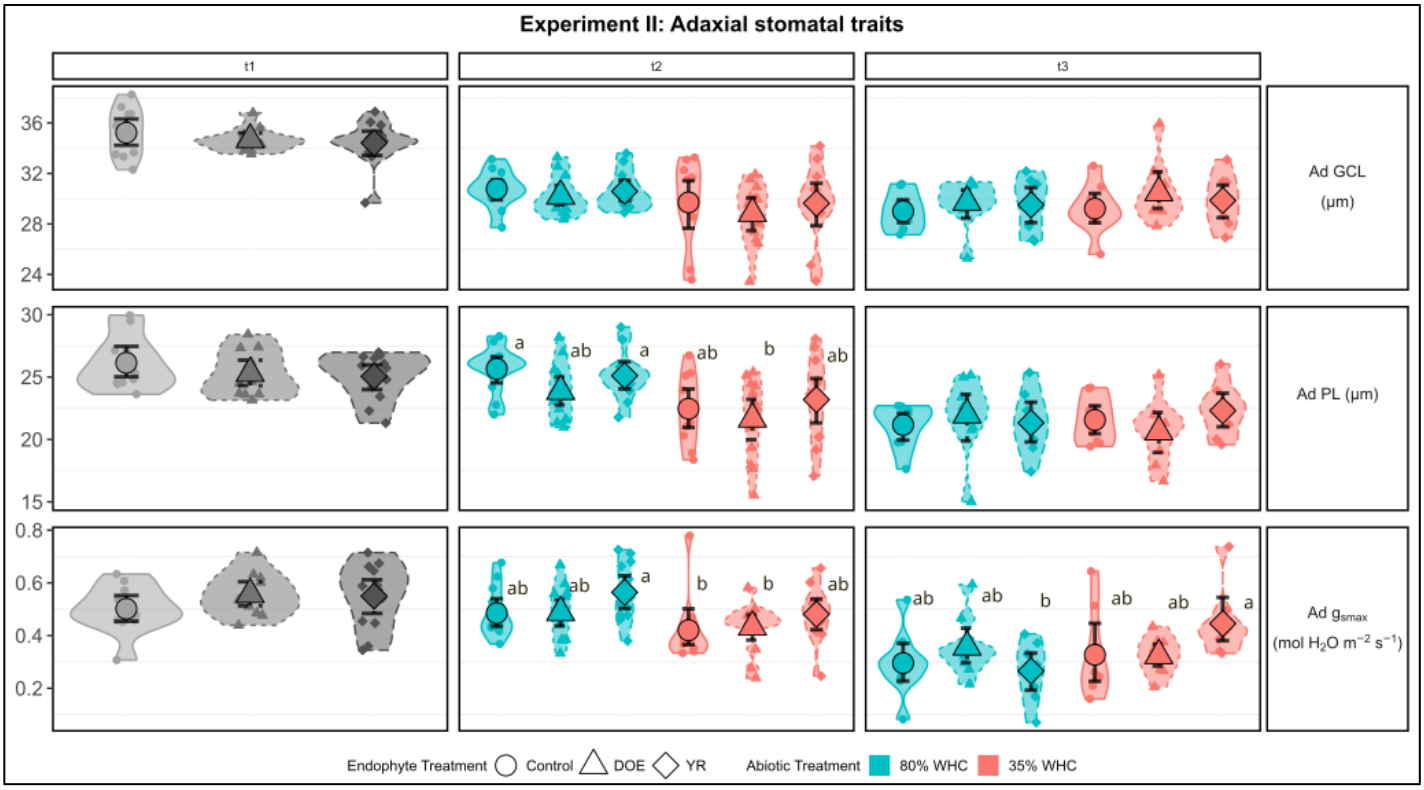

Figure 10. Experiment II: violin plots of adaxial stomatal anatomy from uninoculated (control; circles) and endophyte-inoculated (triangles) *Populus trichocarpa* pre (shaded) and post water-deficit. Blue represents well-watered (80% WHC) and red illustrates water-deficit (35%) soil-moisture conditions. Enlarged shapes represent the mean and lines illustrate the ±95% confidence interval of guard cell length (GCL), pore length (PL), stomatal index (SI), and anatomical maximum stomatal conductance (g_{smax}). Compact letter display (CLD) used to represent significant differences ($P < 0.05$) between treatment means, using the results of Wilcoxon-Mann-Whitney tests for pairwise *post-hoc* tests. Confidence intervals were created from the quantiles of case-resampled bootstrap replicates (n = 1000). Overall effect sizes are given in Table 5.

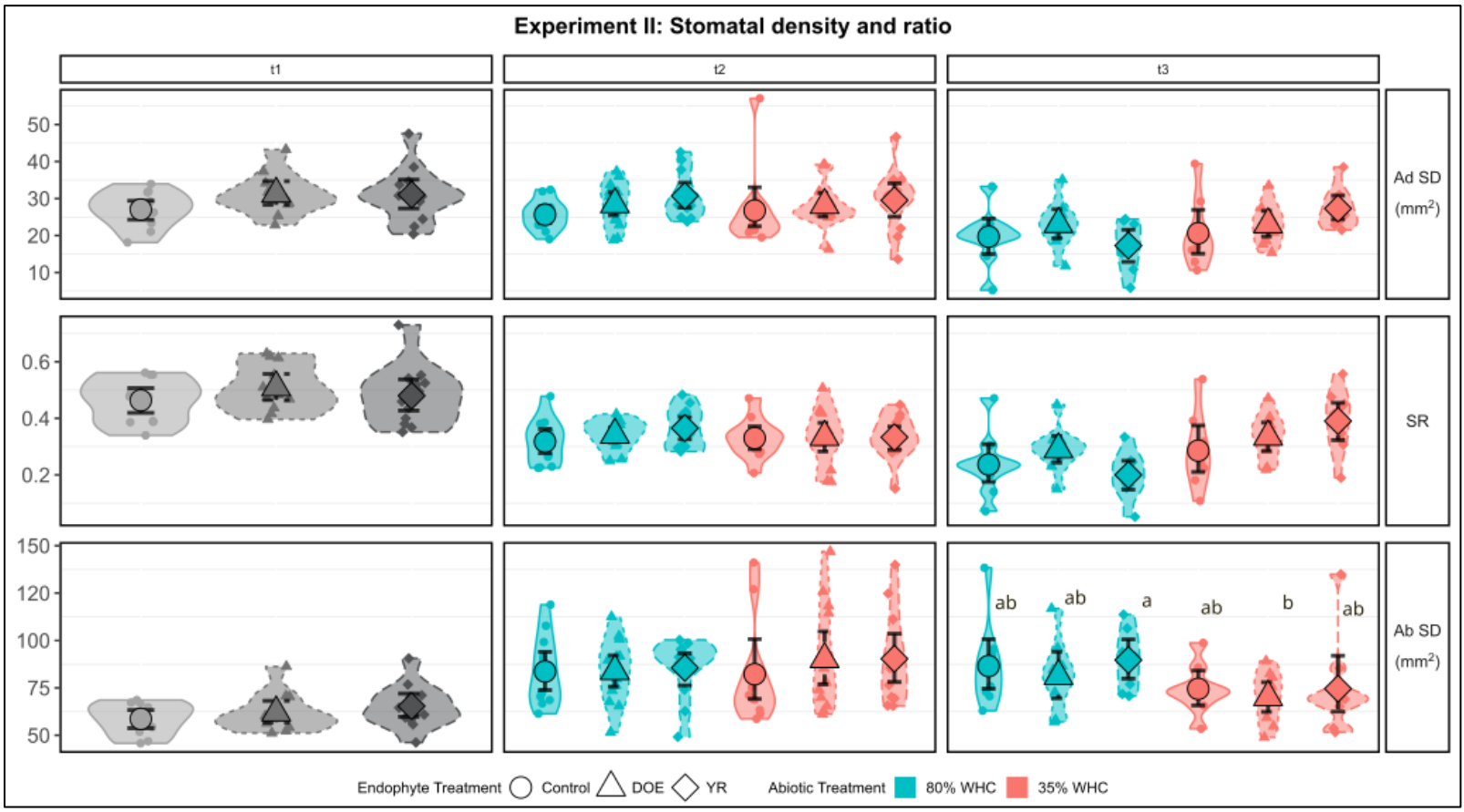

Figure 11. Experiment II: violin plots of adaxial (top row) and abaxial (bottom row) stomatal densities (SD), and their ratios (SR; middle row) from uninoculated (control; circles) and endophyte-inoculated (triangles) *Populus trichocarpa* pre (shaded) and post water-deficit. Blue represents well-watered (80% WHC) and red illustrates water-deficit (35%) soil-moisture conditions. Enlarged shapes represent the mean and lines illustrate the ±95% confidence interval of stomatal density (SD) and stomatal ratio (SR). Compact letter display (CLD) used to represent significant differences ($P < 0.05$) between treatment means, using the results of Wilcoxon-Mann-Whitney tests for pairwise *post-hoc* tests. Confidence intervals were created from the quantiles of case-resampled bootstrap replicates (n = 1000). Overall effect sizes are given in Table 5.

4 Discussion

4.1 Interpretation

4.1.1 Overview

The results of the two greenhouse studies both supported and deviated from the initial hypotheses. Inoculated *Populus trichocarpa* displayed higher intrinsic water-use efficiency (*iWUE*) under light saturation (2000 $\mu mol_{photons}\, m^{-2}\, s^{-1}$) during the water deficit by maintaining assimilation (A_{net}) and lowering stomatal conductance (g_{sw}). Endophyte consortia from two river systems on the west side of the Cascades holistically altered the leaf stomatal patterning during experiment I, driven by changes in stomatal size and density. However, the consortia's variable influence between observations and lack of effect in Experiment II performed in autumn warrants investigation. Notable correspondence between compositional stomatal traits and operational g_{sw} highlighted the importance of morphology, but the unexplained variation implies stomatal dynamics plays an influential role.

4.1.2 Endophytes improve iWUE of Populus trichocarpa under high light

We hypothesized inoculation to improve *iWUE* (A_{net}/g_{sw}) under high light after experiencing a soil-moisture deficit. Our leaf-gas exchange data supported this, showing improvements in *iWUE* at light saturation (**Table 4**; **Fig 5**), consistent with previous studies that used Salicaceae endophytes in black cottonwood and other species (Banan et al., 2023; Khan et al., 2016; Rho et al., 2018). These enhancements after the water stress were driven by reductions in g_{sw} and maintenance of A_{net}. Our results differed than the previous study with black cottonwood as the decreases of g_{sw} from inoculation did not depend on soil-moisture status

(Banan et al., 2023). However, the effect was more pronounced during the water-deficit (**Table 4**). This physiological response depends on specific signals generated by the endophytes of microbes and their interactions with other abiotic factors (Melotto et al., 2017).

One pathway to interpret these observations involves phytohormones. Certain Salicaceae endophyte strains used in this experiment, such as WP1, PTD1, WP5, and WW5 (**Table 2**), have shown to generate abscisic acid (ABA), brassinosteroids (BR), gibberellic acid (GA), indole-3-acetic acid (IAA), jasmonates (JA), and salicylic acid (SA; Kahn et al. 2016). These hormones are involved in the complex crosstalk that affects stomatal movement, and apart from IAA and a specific jasmonate (JA-Ile), all generally can promote stomatal closure (Acharya & Assmann, 2009; Melotto et al. 2017). Though black cottonwood and related hybrids have shown limited stomatal sensitivity to ABA (Marron et al., 2014; Ridolfi & Dreyer, 1997), this hormone still promotes solute leakage from guard cells (Schulte & Hinckley, 1987). Assuming the endophytes increase leaf ABA content *in vivo*, as seen in rice (Rho et al. 2018c), the higher accumulation may lead to osmotic adjustments of the guard cells over time, resulting in reduced stomatal aperture and conductance. However, future research may need to confirm the presence and timing of ABA concentrations within inoculated black cottonwood leaves. In addition, the role of other hormones can be investigated to untangle the most important cascading signals from endophytes that lead to stomatal closure.

We also observed that inoculated plants experienced a lower *iWUE* at light saturation before the water stress due to a reduction of A_{net} and A_{max} (**Table 4; Fig 3 - 5**). Over time, these returned to values matching those of uninoculated plants, suggesting a state of equilibrium between host and endophyte (**Fig 3 -4**). As carbon assimilated is eventually partitioned to different sinks for plant growth, tissue maintenance, or hosting microbe and endophytes, this

early limitation may represent the cost to establish symbiosis (Kiers & Denison, 2008; Rho et al., 2018a). At a whole-plant level, previous studies have noted this carbon expense by observing an initial suppression of growth after establishing these host-consortia symbioses in hybrid poplar (Knoth et al., 2014) and conifers (Aghai et al., 2019). However, the dynamics of carbon partitioning in plant-endophyte relationships remain largely unexplored (Rho & Kim, 2017), and future efforts may examine the timing of the switch from being carbon costly to neutral.

4.1.3 Inoculation alters trends in stomatal morphology and overall patterning

We hypothesized that inoculation would change trends of stomatal patterning and reveal a collective difference between treatments. Unless explicitly noted, this section refers to experiment I. Experiment II is discussed further in *Inconsistencies between experiment I & II*.

Inoculation with the DOE mix of endophytes significantly reduced guard cell and pore length before and during the water-deficit, with less consistent effects on other individual traits (**A6-A9**). Across diverse plant species, reports have observed increases in stomatal length from different endophytes (Larraburu et al., 2010; Romana et al., 2016; Hu et al., 2021). Notably, the presence of the fungal endophyte, *Metarhizium robertsii*, corresponded to decreases in leaf ABA concentrations of the common bean (*Phaseolus vulgaris*), and the authors attributed this to the greater stomatal length (Hu et al., 2021). While exact comparisons remain challenging due to functional differences of these organisms, this highlights the importance of the signals that underpin plant-microbe relationships. The driving theory behind this study stemmed from the assumption that Salicaceae endophytes may share pathways that could elicit a stomatal defense response (Carvahlo et al. 2016, Melotto et al., 2017). Though lacking explicit empirical connections, it relied on the previous *in vivo* and *in vitro* findings that showed endophytes

promote hormones involved in inhibiting stomatal development (Kahn et al., Rho et al., 2018c). As the results from experiment II showed no effect from inoculation on stomatal size (**Fig 12-14**) and experiment I saw highly variable results within sampling timepoints (**A6-A8**), this may warrant additional studies to determine the timing of the signals, such as *in vivo* leaf hormone assays.

Prior to the water-stress, inoculation with the DOE Mix of endophyte strains showed trends of increased stomatal numbers on both leaf surfaces (**Fig 6**) and had a marginally significant effect on abaxial numbers post water-deficit (**Table 4; Fig 8**). This deviates from previous work that has shown lower abaxial stomatal densities in both inoculated rice (Rho et al., 2018c) and apple (Rho et al., 2020a). Direct comparisons of these results remain challenging due to the different biological systems, experimental contexts, and uncertainties revolving around methods. For example, ABA was suggested as a potential driver of lower numbers, but several other hormones crosstalk to regulate stomatal proliferation (Wei et al., 2021). In black cottonwood, various pathways have been identified that alter stomatal density and future efforts could identify the effect of these consortia on these mechanisms (Mckown et al. 2014; Mckown et al., 2019; Chhetri 2020).

Although insignificant when examined individually, inoculated plants tended to have lower stomatal ratios from less adaxial leaf stomata under well-watered conditions, but this effect was not seen for the inoculated plants experiencing a water deficit (**A10-12**). Assuming again that endophytes may elicit similar responses in plants as pathogens (Carvahlo et al., 2016), shifts in stomatal ratios can be interpreted through a cost-benefit theory where a drop in adaxial numbers lowers the chance of foliar pathogen attacks at the expense of a reduced leaf gas-exchange (Muir et al., 2015; Mckown et al., 2019). This would align with empirical research in

black cottonwood that has observed decreases in stomatal ratio along a latitudinal moisture gradient that corresponds with longer growing seasons and higher disease incidence (Mckown et al., 2014; Mckown et al., 2019). Notably, adaxial density and stomatal ratio tended to increase with water-deficits as seen in this study (**A9-A11**), which negated any observed shift in stomatal ratio from inoculation (**Fig 7**). This increase in adaxial density and ratios has been observed in previous studies that examined both climatic dryness and soil moisture levels on stomatal numbers (Dunlap et al., 2001; Pearce et al., 2006; Mckown et al. 2014). One explanation for this observation is that the influence of abiotic stress could overcome the signals from the endophytes (Melotto et al., 2017). Future work may examine if endophytes influence the expression of *PtSPCH1* – an important poplar homologue that determines stomatal distribution (Mckown et al., 2019)

The accumulation of these changes showed an overall difference in stomatal patterning from inoculation with the DOE Mix (**A13**). Inoculated plants tended to have denser, smaller stomata in addition to greater anatomical g_{smax} (**Fig 6).** However, variation existed for each trait and overall patterning at various times along the moisture deficit (**A10 – 12; A16**). Inoculation could only explain about a fifth of the variation in overall differences between treatments (**Fig 6**), suggesting other important drivers underlying this change. For example, our blocking terms explained relatively large amounts of variation ($0.18 \leq R^2 \leq 0.24$), which may reflect the impact of the different temperature or humidity experienced by the plants due to their spatial arrangement in the greenhouse. However, it is challenging to pinpoint the exact effect this would have on stomatal development as the greater literature has no consensus on the impact of humidity on stomatal patterning (Bertolino et al., 2019).

4.1.4 Stomatal patterning corresponds to leaf-gas exchange

We hypothesized that variations in stomatal patterning would correspond to differences in g_{sw} seen at high light. To test this, we used a principal component regression (PCR) model that represented the 13 stomatal traits, and this related to g_{sw} under high light before ($R^2_{adjusted}$ = 0.24; p = 0.1) and after water-deficit ($R^2_{adjusted}$ = 0.63; p = 0.002). The analysis showed a significant relationship between g_{sw} and PC1, which represented stomatal density and size (**Fig 8**). The direction of this relationship indicated that as operational g_{sw} increased, the magnitude of the PC scores representing plants with larger, sparser stomata and lower anatomical g_{smax} also increased. The plants were distributed along a continuum, with distinct clusters based on treatment (**Fig 8**). Specifically, uninoculated well-watered plants showed the largest, least dense stomata, resulting in the highest g_{sw} values, while inoculated water-deficit plants displayed the lowest g_{sw} with smaller, dense stomata.

The biomechanics of this relationship could depend on the relative importance of interconnected processes that relate structure to function. Smaller stomata can respond quicker to signals due to a greater membrane surface area to volume ratio of the guard cells (Drake et al., 2013). This would lead to a faster exchange of solutes between adjacent cells and therefore the opening and closing of the pores (Franks & Farquhar 2007). Additionally, denser stomata may indicate more tightly packed cells across the epidermis, which could increase the mechanical advantage over the guard cells, potentially limiting a greater aperture (Dow et al., 2014). This could be amplified by overlapping diffusion shells that would reduce transpiration (Lehmann & Or, 2015). However, considering only the biomechanical effect ignores physiological impacts, like osmotic shuffling or other active processes that could alter the stomatal response. While the

exact signals from inoculation that could lead to these shifts in relation to environmental conditions remains unclear, it may involve the interplay between biomechanical processes, hormonal changes, and other physiological functions. As dynamic processes have an important role in endophyte-host symbioses, this drove an investigation into the short-term responses of stomata relation to *iWUE*.

To perform this, we followed previously developed protocols (McAusland et al., 2016; Durand et al., 2019). Briefly, this involved adapting a leaf in the chamber to a low light condition (100 $\mu mol_{photon}\, m^{-2}\, s^{-1}$) before directly increasing the light level (2000 $\mu mol_{photon}\, m^{-2}\, s^{-1}$) and measuring g_{sw} every minute for 90 minutes. However, the results showed relatively little variation to changing light (data not shown). This less pronounced stomatal response aligns with observations in wild black cottonwood, which exhibits reduced stomatal activity during Autumn (Cuelmans & Impens, 1988). Our observations took place in late October, coinciding with the period when black cottonwood tends to move towards dormancy, which could account for the reduced stomatal responsiveness (Cuelmans & Impens, 1988). However, it is possible that the controlled conditions of the greenhouse, such as the supplemental lighting, and clonal propagation may have also influenced these responses, but its extent remains unclear. Future efforts should consider these effects when examining the dynamic stomatal response.

4.1.5 Scaling iWUE to whole-plant WUE

Building on the previous discussion, the changes in leaf physiology and morphology from inoculation may extend to whole-plant water use efficiency (*WUE*). Our results show that endophyte inoculation could reduce stomatal size and increase density in black cottonwood, and this related to increases in *iWUE* at high light at the leaf level (**Table 4***)*. However, instantaneous leaf-level water-use efficiency does not always translate to the whole plant scale due in part to

the complex relationship between canopy architecture and microclimate (Medrano et al., 2015; Leakey et al., 2019). In previous work with Salicaceae endophytes and black cottonwood, no relationship was found between these parameters (Banan et al., 2023). This is further complicated by the uncertainty of inoculation effects associated with diurnal light levels (Rho et al., 2018c; Banan et al. 2023). One approach could integrate *iWUE* over the course of the day, but this still generates variable results partly because of leaf position in relation to light (Medrano et al., 2015).

Alternatively, one pathway may incorporate scaling relationships between stomata morphology and other leaf traits, such as mesophyll anatomy and specific leaf area (SLA). For example, in black cottonwood, stomatal density has shown to inversely correlate with SLA (Afas et al., 2006) and directly with biomass accumulation (Afas et al., 2007). Assuming this relationship holds true across studies, this could generate a hypothesis that inoculation may confer a unique leaf phenotype that would conserve water through less transpirational area (i.e., lower SLA) and greater biomass. Further mechanistic hypotheses could be based on these relationships; however, some remain less understood, such as leaf mesophyll anatomy and amphistomy (Drake et al., 2019). A morphometric approach may address these gaps and contribute to a comprehensive understanding of the inoculation effect in determining water use efficiency of the whole plant.

4.1.6 Inconsistencies between Experiment I & II

While experiment I showed numerous significant effects of inoculation on host stomatal anatomy and leaf-gas exchange (**A9**), experiment II showed no effect. This was assumed to be from failed endophyte colonization; however, this theory remains unconfirmed (see future

directions). A suite of endophyte strains were added, and depending on their colonization success, these could have a range of distinct impacts on the host. While unsuccessful colonization may offer a parsimonious explanation for lack of treatment effects, many reasons can underpin this, and two potential factors were considered. First, the seasonal light differences could have affected the rate of photosynthesis, decreasing the available carbohydrates below a threshold necessary maintain symbiosis (**Table 3**; Davitt et al., 2010; Heath et al., 2020). However, this explanation remains unconvincing as Salicaceae endophytes have shown beneficial effects in rice under similar conditions (Rho et al., 2018c).

Another possible reason for the lack of an endophyte signal was an apparent disease pressure. Although not quantified, powdery mildew was noted on plant surfaces throughout the experiment, and these pathogens may have limited endophyte colonization success. When defending against pathogens, the immune response of a plant can be upregulated to exclude endophytes. One morphological piece of evidence to support the presence of pathogens was the drop in stomatal ratio from a decrease in adaxial densities seen across plants, regardless of inoculation status (**Table 5**; **Fig 14**). This follows the same theory as described previously about black cottonwood reducing stomatal ratio to avoid higher disease incidence (Mckown 2019).

4.2 Limitations and future directions

Although drawing conclusions based on the results of a single greenhouse experiment limits the scope of this work, this study contributes to our understanding of endophyte effects on stomatal development and leaf gas-exchange. Endophyte inoculated plants showed decreases in stomatal size with increasing trends in density and g_{smax} that linked to a lower conductance and increase in intrinsic water-use efficiency (*iWUE*). Improving *iWUE* of trees, such as black

cottonwood, in silviculture industries remains a target (Biselli et al., 2022), and using endophytes could be a novel way to achieve this goal.

However, plant-endophyte interactions highly depend on context, and the lack of clear results in experiment II support this claim (Rho & Kim 2017). The major implications of this study exist in guiding future research directions and highlighting the importance of clear hypothesis-driven experiments when examining endophyte interactions. To realize the benefits of these consortia, future efforts may focus on addressing the unknowns of this study, such as quantifying the microbiome and exploring the underlying mechanisms of endophyte-host signaling.

4.2.1 Experimental limitations and improvements

One apparent experimental limitation was the inability to quantify the specific endophyte strains used in the inoculation treatment. Though previous work has successfully shown inoculated plants have higher colony forming unit (CFU) counts (Rho et al., 2018a; Rho et al., 2018c)., this method has been inconsistent in recent experiments, due to the time plants spend in the unsterile greenhouse (data not shown). To address this limitation in future studies, more precise quantification of specific endophytes could be achieved by using droplet digital polymerase chain reactions (ddPCR) with strain-specific primers (Taylor et al., 2017).

Another experimental limitation was the unevenness in the experimental water-deficit, particularly evident in experiment I (**Fig 1**). In experiment II, the frequency of fertigation was increased, and this was likely the reason for improving precision of the water-holding capacity (**Table 3**). The effects of this were noted by comparing the scales and variability of stomatal

traits between experiments (**Fig 14**; **A12**). Further, the variability in stomatal traits between sampling timepoints may have been influenced by the progression of the water-deficit, in addition to other confounding factors. As stomatal patterning showed minor changes over time, the decision to aggregate sampling timepoints was done to potentially stabilize noise, simplify the analysis, and investigate longer term trends. However, it should be noted that this likely reduced the temporal resolution and dynamic causality underlying the relationship between stomatal patterning and conductance. Additionally, standardizing the examined leaves using the leaf plastichron index may help reduce variability between observations, although it requires more time and effort (Larson and Isebrands, 1971). Accounting for plant biomass in calculating the water-deficit progression could also improve the precision of estimated water-holding capacity, particularly as the plant grows. Future experiments may consider using biomass and height data to establish allometric relationships, enhancing water status estimates.

4.2.1.1 Sampling limitations and improvements

Sampling and analyzing stomatal morphological traits, such as size, number, and distribution, was labor-intensive and time-consuming in this study. While both experiments benefited from computer vision, which saved hundreds of hours of manual photo processing, imaging stomatal impressions was the rate-limiting step across both experiments. Reviewing the literature showed wide variability in the techniques used for sampling and processing stomatal data. For example, some authors studying *Populus spp*. covered small areas for imaging stomatal density (0.21 mm^2; Mckown et al., 2014), while others would cover a larger area (3.44 mm^2) (Mckown et al., 2014; Durand et al., 2019). In this paper, we aimed to minimize variation within subsamples by increasing the examined leaf area or the number of measured sub-replicates. Comparing the influence of image magnification on stomatal data collection, we found that

smaller fields of view tended to overestimate calculated values that involve count data compared to data collected from reduced magnification (data not shown). Further, the observed pore width (PW) in this study highly depended on the focus of an image. Most images had variable focus relative to one another, and minor deviations of this would result in apparent changes to stomatal width. Though this was not quantified, future work should consider its effects. This information can serve as a guide for those interested in empirical stomatal morphology research when designing experiments. Although the trained machine learning models will serve as useful tools in future, a large advancement may come from high resolution, handheld cameras that can effectively remove the step of making and imaging impressions.

Initially, stomatal index calculations were meant to be automated using the image segmentation model trained using RootPainter (Smith et al. 2022), but time constraints halted this process. Future endeavors seeking to automate this sampling procedure should train a model with StomataGsmax as it allows feature extraction of multiple image layers (Gibbs et al., 2021) Although this approach would require upfront annotation of images with the Pixel Annotation Tool (Bréhéret, 2017) and iterations of model training and validation, it will likely save substantial time compared to manual counting using the Cell Counter plugin in ImageJ. The ideal model would be able to determine density, size, and index from high resolution images (3584 x 2786 pixels) that cover large areas (1.104 mm^2/image, equivalent to one photo taken at 100x magnification).

4.2.2 Analytical limitations and improvements

One potential limitation in our analysis was categorizing inoculated plants as a presence or absence variable. Quantifying the microbiome, specifically the strains used in this experiment,

would allow follow-up analyses that may provide convincing evidence of the relationship between endophyte abundance and plant physiology. These could take the form of 1) mechanistic modeling or 2) either multivariate indicator species analysis (ISA) or threshold indicator taxa analysis (TITAN). The latter approach has successfully corresponded microorganism composition with leaf traits or environmental conditions (Yan et al., 2022; McBurney et al. 2017) and may have potential in this research by repurposing the approach to examine endophyte abundance in relation to stomatal patterning or other physiological traits.

4.2.2.1 Empirical Modeling

This study generated new composite variables to correspond stomatal morphology with conductance, based on highly correlated individual stomatal traits. One argument against this technique is that it can obscure the biological meaning of the relationships under investigation. In this case, we leveraged a widely observed inverse relationship between stomatal size and number to produce composite variables that could avoid the statistical pitfalls but maintain interpretation (Lertnigm et al., 2022; Franks & Beerling, 2009). However, an alternative approach could have applied multiple regression analysis by examining all combinations of stomatal traits with iterations of model selection or averaging. This could take the form of structural equation modeling, which has been successfully used in stomatal biology (Muir 2018). Traits implemented in the models for this study were chosen based on biological assumptions that met the criteria for the research questions, but further analysis could determine the relative importance of predictors through a method of partitioning R^2 (Tonidandel & LeBreton, 2011).

4.2.2.1 Repeated Measures

Except for adaxial guard cell length, time did not have an interactive effect with inoculation on stomatal traits (**A9**). However, examining the treatment effects within each timepoint showed sometimes inexplicable effects. This could be due to a variety of reasons. For example, stomatal traits are highly variable between and within leaves. It would take a highly standardized procedure to minimize all sources of variation to more accurately capture this within time effect. From this experiment, the lack of endophyte effects over time suggests analyzing the repeated samples of stomatal impressions in future endophyte experiments with black cottonwood may not be necessary. Further, the consistent inoculation effect on leaf side may suggest little need to work on both leaf surfaces. However, this could be affected by different experimental factors like setting or abiotic stress.

5 Conclusion

This study supported previous results and explored new questions regarding the influence of Salicaceae endophytes on intrinsic water-use efficiency (*iWUE*) in black cottonwood (*Populus trichocarpa*) under water stress. Our findings generated insight into the complex interactions of plants, endophytes, and abiotic stress, giving insight for future research.

Through the first greenhouse experiment, we reaffirmed the ability of Salicaceae endophytes to improve *iWUE* in black cottonwood under high light during water stress. These improvements corresponded to underlying shifts in stomatal patterning, characterized by smaller guard cells and pores. However, there were discrepancies between experiments, which may have been due to failed colonization, influenced by factors like disease pressure. Addressing these problems and understanding the nuances of endophyte-host relationships will be critical for future research in this field.

In conclusion, this paper contributes to the understanding of plant-microbe interactions, its influence on stomatal development, and its relation on leaf gas-exchange, highlighting the potential for harnessing mutualistic partnerships to improve water-use efficiency in commercially valuable trees. Moving forward, more comprehensive studies using advanced techniques for quantifying endophyte strains and controlled experimental designs will deepen the insights into mechanisms underlying the complex interactions. These are promising advancements for enhancing water-use efficiency and sustainable productivity in forest systems, contributing to the larger efforts in alleviating the impacts of climate change.

Bibliography

Acharya, B. R., & Assmann, S. M. (2009). Hormone interactions in stomatal function. *Plant Molecular Biology*, *69*(4), 451–462. https://doi.org/10.1007/s11103-008-9427-0

Aghai, M. M., Khan, Z., Joseph, M. R., Stoda, A. M., Sher, A. W., Ettl, G. J., & Doty, S. L. (2019). The Effect of Microbial Endophyte Consortia on Pseudotsuga menziesii and Thuja plicata Survival, Growth, and Physiology Across Edaphic Gradients. *Frontiers in Microbiology*, *10*, 1353. https://doi.org/10.3389/fmicb.2019.01353

Al Afas, N., Marron, N., & Ceulemans, R. (2006). Clonal variation in stomatal characteristics related to biomass production of 12 poplar (Populus) clones in a short rotation coppice culture. *Environmental and Experimental Botany*, *58*(1–3), 279–286. https://doi.org/10.1016/j.envexpbot.2005.09.003

Anderson, M. J. (2001). A new method for non-parametric multivariate analysis of variance: NON-PARAMETRIC MANOVA FOR ECOLOGY. *Austral Ecology*, *26*(1), 32–46. https://doi.org/10.1111/j.1442-9993.2001.01070.pp.x

Anderson, M. J. (2017). Permutational Multivariate Analysis of Variance (PERMANOVA). In N. Balakrishnan, T. Colton, B. Everitt, W. Piegorsch, F. Ruggeri, & J. L. Teugels (Eds.), *Wiley StatsRef: Statistics Reference Online* (1st ed., pp. 1–15). Wiley. https://doi.org/10.1002/9781118445112.stat07841

Augusto, L., & Boča, A. (2022). Tree functional traits, forest biomass, and tree species diversity interact with site properties to drive forest soil carbon. *Nature Communications*, *13*(1), 1097. https://doi.org/10.1038/s41467-022-28748-0

Biselli, C., Vietto, L., Rosso, L., Cattivelli, L., Nervo, G., & Fricano, A. (2022). Advanced Breeding for Biotic Stress Resistance in Poplar. *Plants*, *11*(15), 2032. https://doi.org/10.3390/plants11152032

Boer, H. J., Price, C. A., Wagner-Cremer, F., Dekker, S. C., Franks, P. J., & Veneklaas, E. J. (2016). Optimal allocation of leaf epidermal area for gas exchange. *New Phytologist*, *210*(4), 1219–1228. https://doi.org/10.1111/nph.13929

Buckley, T. N. (2019). How do stomata respond to water status? *New Phytologist*, *224*(1), 21–36. https://doi.org/10.1111/nph.15899

Carvalho, T. L. G., Ballesteros, H. G. F., Thiebaut, F., Ferreira, P. C. G., & Hemerly, A. S. (2016). Nice to meet you: genetic, epigenetic and metabolic controls of plant perception of beneficial associative and endophytic diazotrophic bacteria in non-leguminous plants. *Plant Molecular Biology*, *90*(6), 561–574. https://doi.org/10.1007/s11103-016-0435-1

Chhetri, H. B., Furches, A., Macaya-Sanz, D., Walker, A. R., Kainer, D., Jones, P., Harman-Ware, A. E., Tschaplinski, T. J., Jacobson, D., Tuskan, G. A., & DiFazio, S. P. (2020). Genome-Wide Association Study of Wood Anatomical and Morphological Traits in Populus trichocarpa. *Frontiers in Plant Science*, *11*. https://www.frontiersin.org/articles/10.3389/fpls.2020.545748

Davitt, A. J., Stansberry, M., & Rudgers, J. A. (2010). Do the costs and benefits of fungal endophyte symbiosis vary with light availability? *New Phytologist*, *188*(3), 824–834. https://doi.org/10.1111/j.1469-8137.2010.03428.x

Doty, S. L. (2017). Functional Importance of the Plant Endophytic Microbiome: Implications for Agriculture, Forestry, and Bioenergy. In S. L. Doty (Ed.), *Functional Importance of the Plant Microbiome* (pp. 1–5). Springer International Publishing. https://doi.org/10.1007/978-3-319-65897-1_1

Doty, S. L., Sher, A. W., Fleck, N. D., Khorasani, M., Bumgarner, R. E., Khan, Z., Ko, A. W. K., Kim, S.-H., & DeLuca, T. H. (2016). Variable Nitrogen Fixation in Wild Populus. *PLOS ONE*, *11*(5), e0155979. https://doi.org/10.1371/journal.pone.0155979

Dow, G. J., Berry, J. A., & Bergmann, D. C. (2014). The physiological importance of developmental mechanisms that enforce proper stomatal spacing in *A rabidopsis thaliana. New Phytologist*, *201*(4), 1205–1217. https://doi.org/10.1111/nph.12586

Drake, P. L., Boer, H. J., Schymanski, S. J., & Veneklaas, E. J. (2019). Two sides to every leaf: water and CO_2 transport in hypostomatous and amphistomatous leaves. *New Phytologist*, *222*(3), 1179–1187. https://doi.org/10.1111/nph.15652

Durand, M., Brendel, O., Buré, C., & Le Thiec, D. (2019). Altered stomatal dynamics induced by changes in irradiance and vapour-pressure deficit under drought: impacts on the whole-plant transpiration efficiency of poplar genotypes. *New Phytologist*, *222*(4), 1789–1802. https://doi.org/10.1111/nph.15710

Firrincieli, A., Khorasani, M., Frank, A. C., & Doty, S. L. (2020). Influences of Climate on Phyllosphere Endophytic Bacterial Communities of Wild Poplar. *Frontiers in Plant Science*, *11*. https://www.frontiersin.org/articles/10.3389/fpls.2020.00203

Flexas, J., Díaz-Espejo, A., Conesa, M. A., Coopman, R. E., Douthe, C., Gago, J., Gallé, A., Galmés, J., Medrano, H., Ribas-Carbo, M., Tomàs, M., & Niinemets, Ü. (2016). Mesophyll conductance to CO_2 and Rubisco as targets for improving intrinsic water use efficiency in C_3 plants: Gm and Rubisco: physiological traits driving WUEi. *Plant, Cell & Environment*, *39*(5), 965–982. https://doi.org/10.1111/pce.12622

Flexas, J., Niinemets, Ü., Gallé, A., Barbour, M. M., Centritto, M., Diaz-Espejo, A., Douthe, C., Galmés, J., Ribas-Carbo, M., Rodriguez, P. L., Rosselló, F., Soolanayakanahally, R., Tomas, M.,

Wright, I. J., Farquhar, G. D., & Medrano, H. (2013). Diffusional conductances to CO2 as a target for increasing photosynthesis and photosynthetic water-use efficiency. *Photosynthesis Research*, *117*(1), 45–59. https://doi.org/10.1007/s11120-013-9844-z

Franks, P. J., & Beerling, D. J. (2009). Maximum leaf conductance driven by CO_2 effects on stomatal size and density over geologic time. *Proceedings of the National Academy of Sciences*, *106*(25), 10343–10347. https://doi.org/10.1073/pnas.0904209106

Frossard, J., & Renaud, O. (2021). Permutation Tests for Regression, ANOVA, and Comparison of Signals: The **permuco** Package. *Journal of Statistical Software*, *99*(15). https://doi.org/10.18637/jss.v099.i15

Gibbs, J. A., Mcausland, L., Robles-Zazueta, C. A., Murchie, E. H., & Burgess, A. J. (2021). A Deep Learning Method for Fully Automatic Stomatal Morphometry and Maximal Conductance Estimation. *Frontiers in Plant Science*, *12*. https://www.frontiersin.org/articles/10.3389/fpls.2021.780180

Harrison, E. L., Arce Cubas, L., Gray, J. E., & Hepworth, C. (2020). The influence of stomatal morphology and distribution on photosynthetic gas exchange. *The Plant Journal*, *101*(4), 768–779. https://doi.org/10.1111/tpj.14560

Hatfield, J. L., & Dold, C. (2019). Water-Use Efficiency: Advances and Challenges in a Changing Climate. *Frontiers in Plant Science*, *10*, 103. https://doi.org/10.3389/fpls.2019.00103

He, M., & Dijkstra, F. A. (2014). Drought effect on plant nitrogen and phosphorus: a meta-analysis. *New Phytologist*, *204*(4), 924–931. https://doi.org/10.1111/nph.12952

Heath, K. D., Podowski, J. C., Heniff, S., Klinger, C. R., Burke, P. V., Weese, D. J., Yang, W. H., & Lau, J. A. (2020). Light availability and rhizobium variation interactively mediate the

outcomes of legume–rhizobium symbiosis. *American Journal of Botany*, *107*(2), 229–238. https://doi.org/10.1002/ajb2.1435

Home | AgWeatherNet at Washington State University. (n.d.). Retrieved July 20, 2023, from https://weather.wsu.edu/

Hu, S., & Bidochka, M. J. (2021). Abscisic acid implicated in differential plant responses of Phaseolus vulgaris during endophytic colonization by Metarhizium and pathogenic colonization by Fusarium. *Scientific Reports*, *11*(1), 11327. https://doi.org/10.1038/s41598-021-90232-4

Kandel, S. L., Herschberger, N., Kim, S. H., & Doty, S. L. (2015). Diazotrophic Endophytes of Poplar and Willow for Growth Promotion of Rice Plants in Nitrogen-Limited Conditions. *Crop Science*, *55*(4), 1765–1772. https://doi.org/10.2135/cropsci2014.08.0570

Khan, A. L., Waqas, M., & Lee, I.-J. (2015). Resilience of Penicillium resedanum LK6 and exogenous gibberellin in improving Capsicum annuum growth under abiotic stresses. *Journal of Plant Research*, *128*(2), 259–268. https://doi.org/10.1007/s10265-014-0688-1

Khan, Z., Guelich, G., Phan, H., Redman, R., & Doty, S. (2012). Bacterial and Yeast Endophytes from Poplar and Willow Promote Growth in Crop Plants and Grasses. *ISRN Agronomy*, *2012*, 1–11. https://doi.org/10.5402/2012/890280

Khan, Z., Rho, H., Firrincieli, A., Hung, S. H., Luna, V., Masciarelli, O., Kim, S.-H., & Doty, S. L. (2016). Growth enhancement and drought tolerance of hybrid poplar upon inoculation with endophyte consortia. *Current Plant Biology*, *6*, 38–47. https://doi.org/10.1016/j.cpb.2016.08.001

Kiers, E. T., & Denison, R. F. (2008). Sanctions, Cooperation, and the Stability of Plant-Rhizosphere Mutualisms. *Annual Review of Ecology, Evolution, and Systematics*, *39*(1), 215–236. https://doi.org/10.1146/annurev.ecolsys.39.110707.173423

Knoth, J. L., Kim, S., Ettl, G. J., & Doty, S. L. (2014). Biological nitrogen fixation and biomass accumulation within poplar clones as a result of inoculations with diazotrophic endophyte consortia. *New Phytologist*, *201*(2), 599–609. https://doi.org/10.1111/nph.12536

Knoth, J. L., Kim, S.-H., Ettl, G. J., & Doty, S. L. (2013). Effects of cross host species inoculation of nitrogen-fixing endophytes on growth and leaf physiology of maize. *GCB Bioenergy*, *5*(4), 408–418. https://doi.org/10.1111/gcbb.12006

Larraburu, E. E., Apóstolo, N. M., & Llorente, B. E. (2010). Anatomy and morphology of photinia (Photinia × fraseri Dress) in vitro plants inoculated with rhizobacteria. *Trees*, *24*(4), 635–642. https://doi.org/10.1007/s00468-010-0433-x

Larson, P. R., & Isebrands, J. G. (1971). The Plastochron Index as Applied to Developmental Studies of Cottonwood. *Canadian Journal of Forest Research*, *1*(1), 1–11. https://doi.org/10.1139/x71-001

Lawson, T., & Blatt, M. R. (2014). Stomatal Size, Speed, and Responsiveness Impact on Photosynthesis and Water Use Efficiency. *Plant Physiology*, *164*(4), 1556–1570. https://doi.org/10.1104/pp.114.237107

Leakey, A. D. B., Ferguson, J. N., Pignon, C. P., Wu, A., Jin, Z., Hammer, G. L., & Lobell, D. B. (2019). Water Use Efficiency as a Constraint and Target for Improving the Resilience and Productivity of C_3 and C_4 Crops. *Annual Review of Plant Biology*, *70*(1), 781–808. https://doi.org/10.1146/annurev-arplant-042817-040305

Lee, H., Calvin, K., Dasgupta, D., & et al. (n.d.). *IPCC, 2023: Summary for Policymakers. Synthesis Report of the IPCC Sixth Assessment Report*. https://www.ipcc.ch/report/ar6/syr/downloads/report/IPCC_AR6_SYR_SPM.pdf

Lehmann, P., & Or, D. (2015). Effects of stomata clustering on leaf gas exchange. *New Phytologist*, *207*(4), 1015–1025. https://doi.org/10.1111/nph.13442

Lertngim, N., Ruangsiri, M., Klinsawang, S., Raksatikan, P., Thunnom, B., Siangliw, M., Toojinda, T., & Siangliw, J. L. (2022). Photosynthetic Plasticity and Stomata Adjustment in Chromosome Segment Substitution Lines of Rice Cultivar KDML105 under Drought Stress. *Plants*, *12*(1), 94. https://doi.org/10.3390/plants12010094

Marron, N., Gielen, B., Brignolas, F., Gao, J., Johnson, J. D., Karnosky, D. F., Polle, A., Scarascia-Mugnozza, G., Schroeder, W. R., & Ceulemans, R. (2014). Abiotic stresses. In J. G. Isebrands & J. Richardson (Eds.), *Poplars and willows: trees for society and the environment* (1st ed., pp. 337–442). CABI. https://doi.org/10.1079/9781780641089.0337

McElwain, J. C., Yiotis, C., & Lawson, T. (2016). Using modern plant trait relationships between observed and theoretical maximum stomatal conductance and vein density to examine patterns of plant macroevolution. *New Phytologist*, *209*(1), 94–103. https://doi.org/10.1111/nph.13579

McKown, A. D., Guy, R. D., Quamme, L., Klápště, J., La Mantia, J., Constabel, C. P., El-Kassaby, Y. A., Hamelin, R. C., Zifkin, M., & Azam, M. S. (2014). Association genetics, geography and ecophysiology link stomatal patterning in *Populus trichocarpa* with carbon gain and disease resistance trade-offs. *Molecular Ecology*, *23*(23), 5771–5790. https://doi.org/10.1111/mec.12969

McKown, A. D., Klápště, J., Guy, R. D., Corea, O. R. A., Fritsche, S., Ehlting, J., El-Kassaby, Y. A., & Mansfield, S. D. (2019). A role for *SPEECHLESS* in the integration of leaf stomatal patterning with the growth vs disease trade-off in poplar. *New Phytologist*, *223*(4), 1888–1903. https://doi.org/10.1111/nph.15911

Medrano, H., Tomás, M., Martorell, S., Flexas, J., Hernández, E., Rosselló, J., Pou, A., Escalona, J.-M., & Bota, J. (2015). From leaf to whole-plant water use efficiency (WUE) in complex

canopies: Limitations of leaf WUE as a selection target. *The Crop Journal*, *3*(3), 220–228. https://doi.org/10.1016/j.cj.2015.04.002

Melotto, M., Zhang, L., Oblessuc, P. R., & He, S. Y. (2017). Stomatal Defense a Decade Later. *Plant Physiology*, *174*(2), 561–571. https://doi.org/10.1104/pp.16.01853

Mordkoff, J. T. (2019). A Simple Method for Removing Bias From a Popular Measure of Standardized Effect Size: Adjusted Partial Eta Squared. *Advances in Methods and Practices in Psychological Science*, *2*(3), 228–232. https://doi.org/10.1177/2515245919855053

Muir, C. D. (2015). Making pore choices: repeated regime shifts in stomatal ratio. *Proceedings of the Royal Society B: Biological Sciences*, *282*(1813), 20151498. https://doi.org/10.1098/rspb.2015.1498

Muir, C. D. (2018). Light and growth form interact to shape stomatal ratio among British angiosperms. *New Phytologist*, *218*(1), 242–252. https://doi.org/10.1111/nph.14956

Qin, X., Zhao, X., Huang, S., Deng, J., Li, X., Luo, Z., & Zhang, Y. (2021). Pest management via endophytic colonization of tobacco seedlings by the insect fungal pathogen *Beauveria bassiana*. *Pest Management Science*, *77*(4), 2007–2018. https://doi.org/10.1002/ps.6229

Rho, H., Doty, S. L., & Kim, S.-H. (2018). Estimating microbial respiratory CO_2 from endophytic bacteria in rice. *Plant Signaling & Behavior*, 1–5. https://doi.org/10.1080/15592324.2018.1500067

Rho, H., Doty, S. L., & Kim, S.-H. (2020). Endophytes alleviate the elevated CO2-dependent decrease in photosynthesis in rice, particularly under nitrogen limitation. *Journal of Experimental Botany*, *71*(2), 707–718. https://doi.org/10.1093/jxb/erz440

Rho, H., Hsieh, M., Kandel, S. L., Cantillo, J., Doty, S. L., & Kim, S.-H. (2018). Do Endophytes Promote Growth of Host Plants Under Stress? A Meta-Analysis on Plant Stress Mitigation by Endophytes. *Microbial Ecology*, *75*(2), 407–418. https://doi.org/10.1007/s00248-017-1054-3

Rho, H., & Kim, S.-H. (2017). Endophyte Effects on Photosynthesis and Water Use of Plant Hosts: A Meta-Analysis. In S. L. Doty (Ed.), *Functional Importance of the Plant Microbiome* (pp. 43–69). Springer International Publishing. https://doi.org/10.1007/978-3-319-65897-1_4

Rho, H., Van Epps, V., Kim, S.-H., & Doty, S. L. (2020). Endophytes Increased Fruit Quality with Higher Soluble Sugar Production in Honeycrisp Apple (Malus pumila). *Microorganisms*, *8*(5), 699. https://doi.org/10.3390/microorganisms8050699

Rho, H., Van Epps, V., Wegley, N., Doty, S. L., & Kim, S.-H. (2018). Salicaceae Endophytes Modulate Stomatal Behavior and Increase Water Use Efficiency in Rice. *Frontiers in Plant Science*, *9*. https://www.frontiersin.org/articles/10.3389/fpls.2018.00188

Ridolfi, M., & Dreyer, E. (1997). Responses to water stress in an ABA-unresponsive hybrid poplar (*Populus koreana* × *trichocarpa* cv. Peace) III. Consequences for photosynthetic carbon assimilation. *New Phytologist*, *135*(1), 31–40. https://doi.org/10.1046/j.1469-8137.1997.00624.x

Rosmana, A., Nasaruddin, N., Hendarto, H., Hakkar, A. A., & Agriansyah, N. (2016). Endophytic Association of *Trichoderma asperellum* within *Theobroma cacao* Suppresses Vascular Streak Dieback Incidence and Promotes Side Graft Growth. *Mycobiology*, *44*(3), 180–186. https://doi.org/10.5941/MYCO.2016.44.3.180

Schneider, C. A., Rasband, W. S., & Eliceiri, K. W. (2012). NIH Image to ImageJ: 25 years of image analysis. *Nature Methods*, *9*(7), 671–675. https://doi.org/10.1038/nmeth.2089

Schulte, P. J., & Hinkley, T. M. (1987). Abscisic acid relations and the response of Populus trichocarpa stomata to leaf water potential. *Tree Physiology, 3*(2), 103–113. https://doi.org/10.1093/treephys/3.2.103

Smith, A. G., Han, E., Petersen, J., Olsen, N. A. F., Giese, C., Athmann, M., Dresbøll, D. B., & Thorup-Kristensen, K. (2022). R OOT P AINTER : deep learning segmentation of biological images with corrective annotation. *New Phytologist*, *236*(2), 774–791. https://doi.org/10.1111/nph.18387

Stanton, B. J., Serapiglia, M. J., & Smart, L. B. (2014). The domestication and conservation of *Populus* and *Salix* genetic resources. In J. G. Isebrands & J. Richardson (Eds.), *Poplars and willows: trees for society and the environment* (1st ed., pp. 124–199). CABI. https://doi.org/10.1079/9781780641089.0124

Stenzel, F., Greve, P., Lucht, W., Tramberend, S., Wada, Y., & Gerten, D. (2021). Irrigation of biomass plantations may globally increase water stress more than climate change. *Nature Communications*, *12*(1), 1512. https://doi.org/10.1038/s41467-021-21640-3

Stevens, James, Faralli, Michele, Wall, Shellie, Stamford, John, & Lawson, Tracy. (2021). Stomatal responses to climate change. In *Photosynthesis, respiration and climate change. Advances in photosynthesis and respiration* (1st ed., Vol. 48, pp. 17–47). Spring Nature. https://repository.essex.ac.uk/30704/

Taylor, S. C., Laperriere, G., & Germain, H. (2017). Droplet Digital PCR versus qPCR for gene expression analysis with low abundant targets: from variable nonsense to publication quality data. *Scientific Reports*, *7*(1), 2409. https://doi.org/10.1038/s41598-017-02217-x

Tonidandel, S., & LeBreton, J. M. (2011). Relative Importance Analysis: A Useful Supplement to Regression Analysis. *Journal of Business and Psychology*, *26*(1), 1–9. https://doi.org/10.1007/s10869-010-9204-3

Urban, J., Ingwers, M. W., McGuire, M. A., & Teskey, R. O. (2017). Increase in leaf temperature opens stomata and decouples net photosynthesis from stomatal conductance in Pinus taeda and Populus deltoides x nigra. *Journal of Experimental Botany*, *68*(7), 1757–1767. https://doi.org/10.1093/jxb/erx052

Vandenkoornhuyse, P., Quaiser, A., Duhamel, M., Le Van, A., & Dufresne, A. (2015). The importance of the microbiome of the plant holobiont. *New Phytologist*, *206*(4), 1196–1206. https://doi.org/10.1111/nph.13312

Wei, H., Jing, Y., Zhang, L., & Kong, D. (2021). Phytohormones and their crosstalk in regulating stomatal development and patterning. *Journal of Experimental Botany*, *72*(7), 2356–2370. https://doi.org/10.1093/jxb/erab034

Wickham, H., Averick, M., Bryan, J., Chang, W., McGowan, L., François, R., Grolemund, G., Hayes, A., Henry, L., Hester, J., Kuhn, M., Pedersen, T., Miller, E., Bache, S., Müller, K., Ooms, J., Robinson, D., Seidel, D., Spinu, V., … Yutani, H. (2019). Welcome to the Tidyverse. *Journal of Open Source Software*, *4*(43), 1686. https://doi.org/10.21105/joss.01686

Yan, K., Han, W., Zhu, Q., Li, C., Dong, Z., & Wang, Y. (2022). Leaf surface microtopography shaping the bacterial community in the phyllosphere: evidence from 11 tree species. *Microbiological Research*, *254*, 126897. https://doi.org/10.1016/j.micres.2021.126897

Appendix

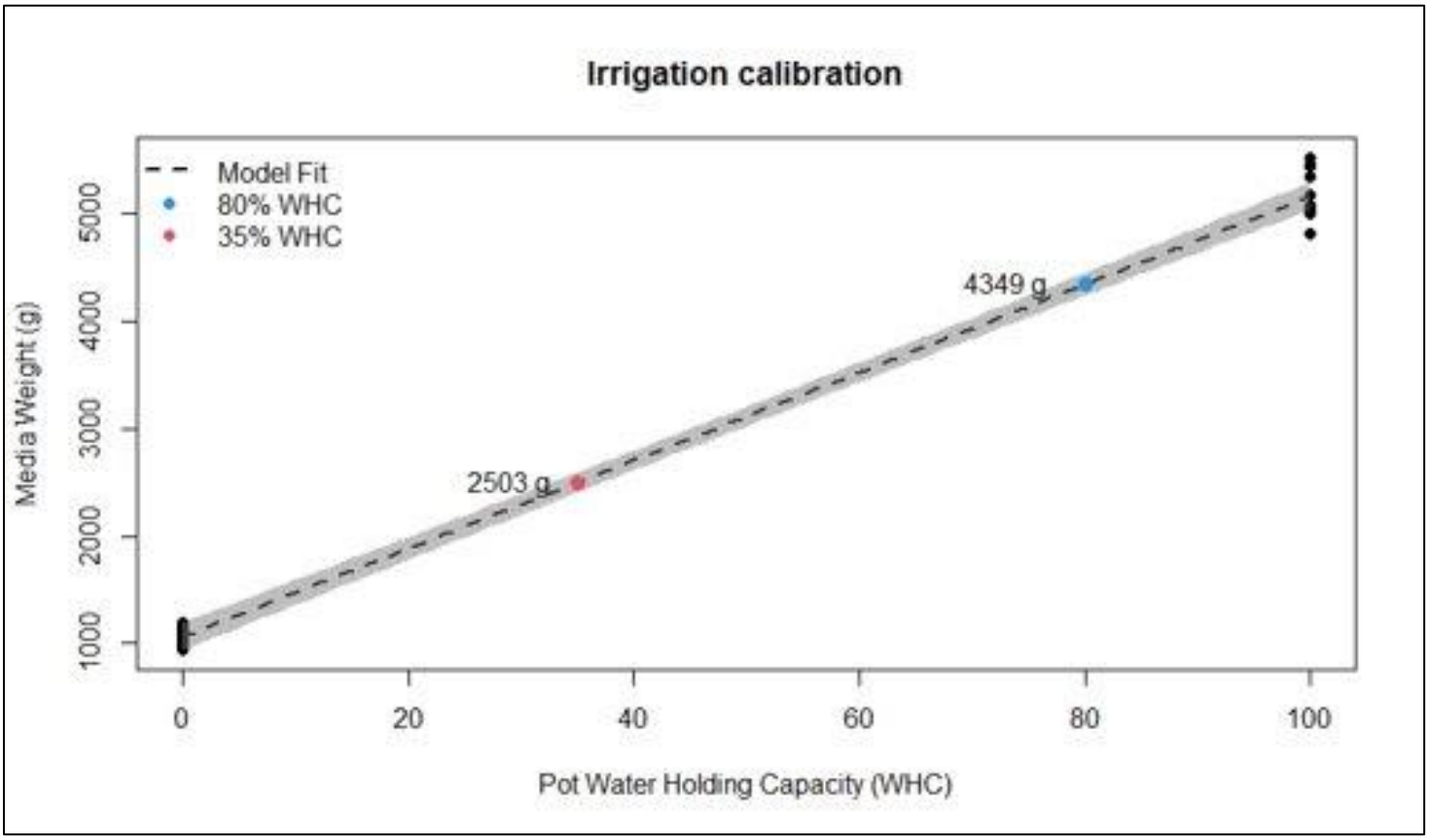

A1. Calibration curve to determine the water-deficit for experiment I. Simple linear regression, fitted with ordinary least squares, was used to convert the mass of potting media to a pot water holding capacity (WHC). Ten 8.5 L pots were filled with 1940 g of media, saturated with water, and covered with plastic wrap to determine the 100 WHC. The same pots were oven-dried to figure out the 0 WHC. While this only represents the calibration curve used in experiment I, experiment II followed the same protocol and looked similar; however, the exact values differed.

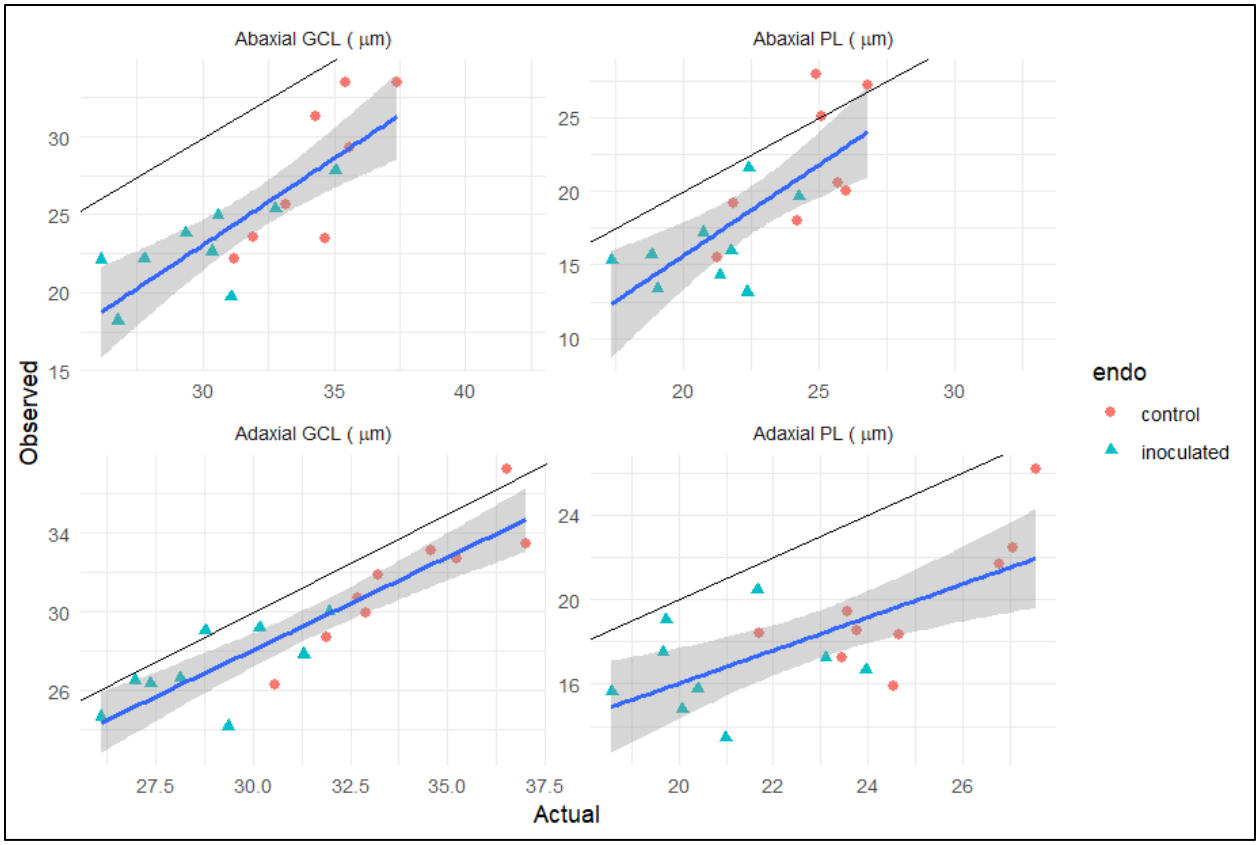

A2. Correspondence of measured stomatal dimensions with those obtained from StomataGSmax (Gibbs et al., 2021). The black line represents the perfect fit of values predicted from the convolutional neural network model (Observed) and those measured manually (Actual). The consistent underprediction (blue line) could detect treatment differences with similar effect sizes as manual measurements; therefore, it was deemed acceptable when comparing treatment differences.

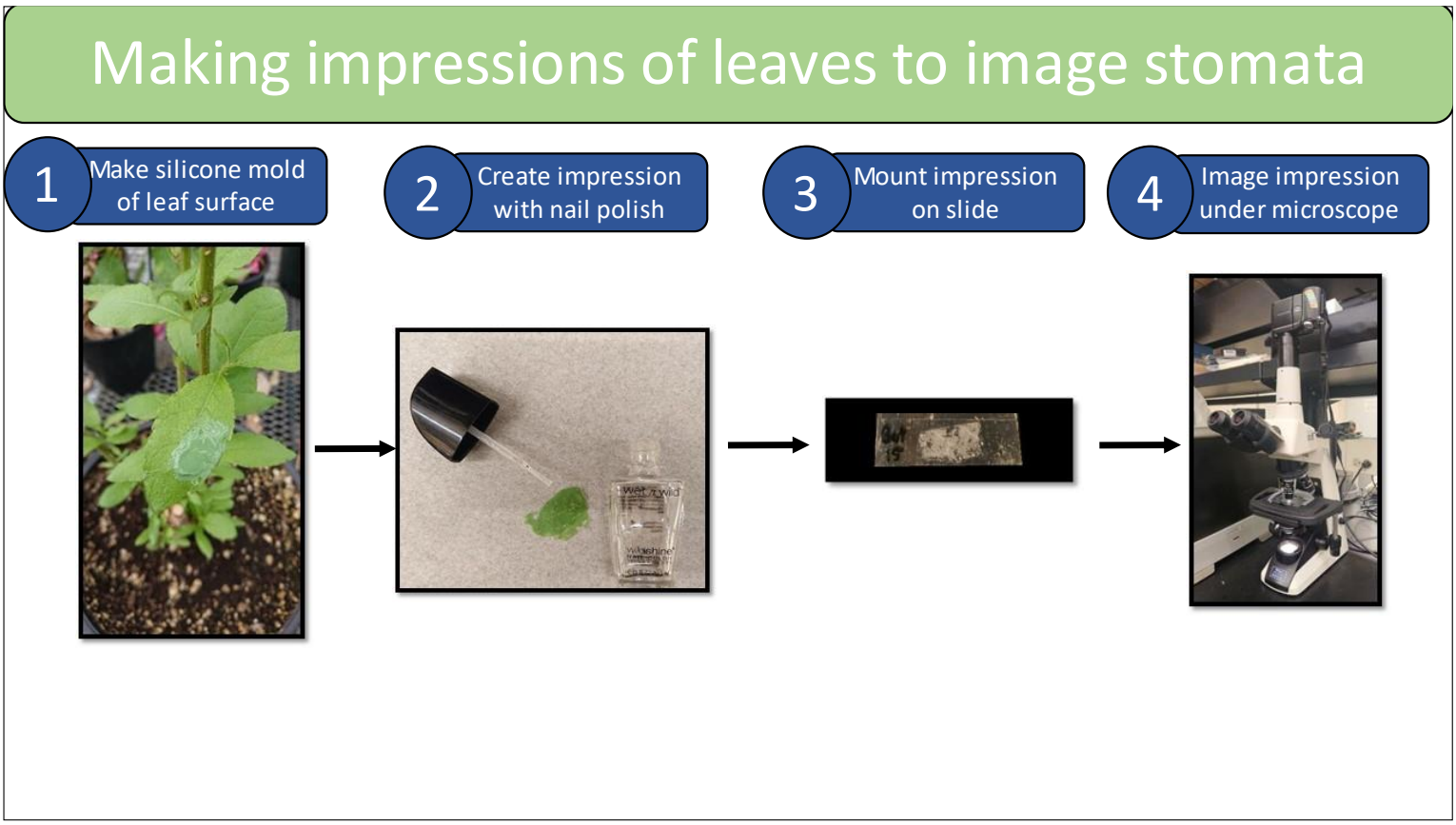

A3. Schematic representation showing the sampling procedure to gather stomatal impressions. Impressions were taken from the youngest, fully expanded, sun exposed leaf, often from the main stem and same area as leaf-gas exchange measurements. This area could be outlined on the leaf by drawing a circle around the gaskets of the gas-exchange system. Putty was dispensed from the cartridge through a mixing tip to combine the catalyst and base of the solution while applying it evenly over the middle of the lamina and away from the midvein. This process was often facilitated using a dispensing gun that could attach to the putty cartridge, but manual mixing and dispensing also works. The putty was allowed to dry into a silicone impression (~5 minutes) before removing it from the leaf. Clear nail varnish was applied on the silicone leaf impressions and allowed to dry (~5 to 60 minutes) before removing the hardened polish with clear adhesive tape (i.e., the positive impression). After mounting the resulting positive impression onto microscope slides, images were taken of each under a microscope using a constant image resolution (1782x1372 pixels). Based on this resolution, the pixel to unit conversion ratio was 6.26 um/pixel for images taken at 400x. However, this should be rechecked for future experiments. At least three images per impression at every time point were taken under 400x magnification (i.e., 0.068 mm^2/image) to measure individual stoma. Four images per impression were taken at every time point under 100x magnification to determine stomatal density (i.e., 1.104 mm^2/image).

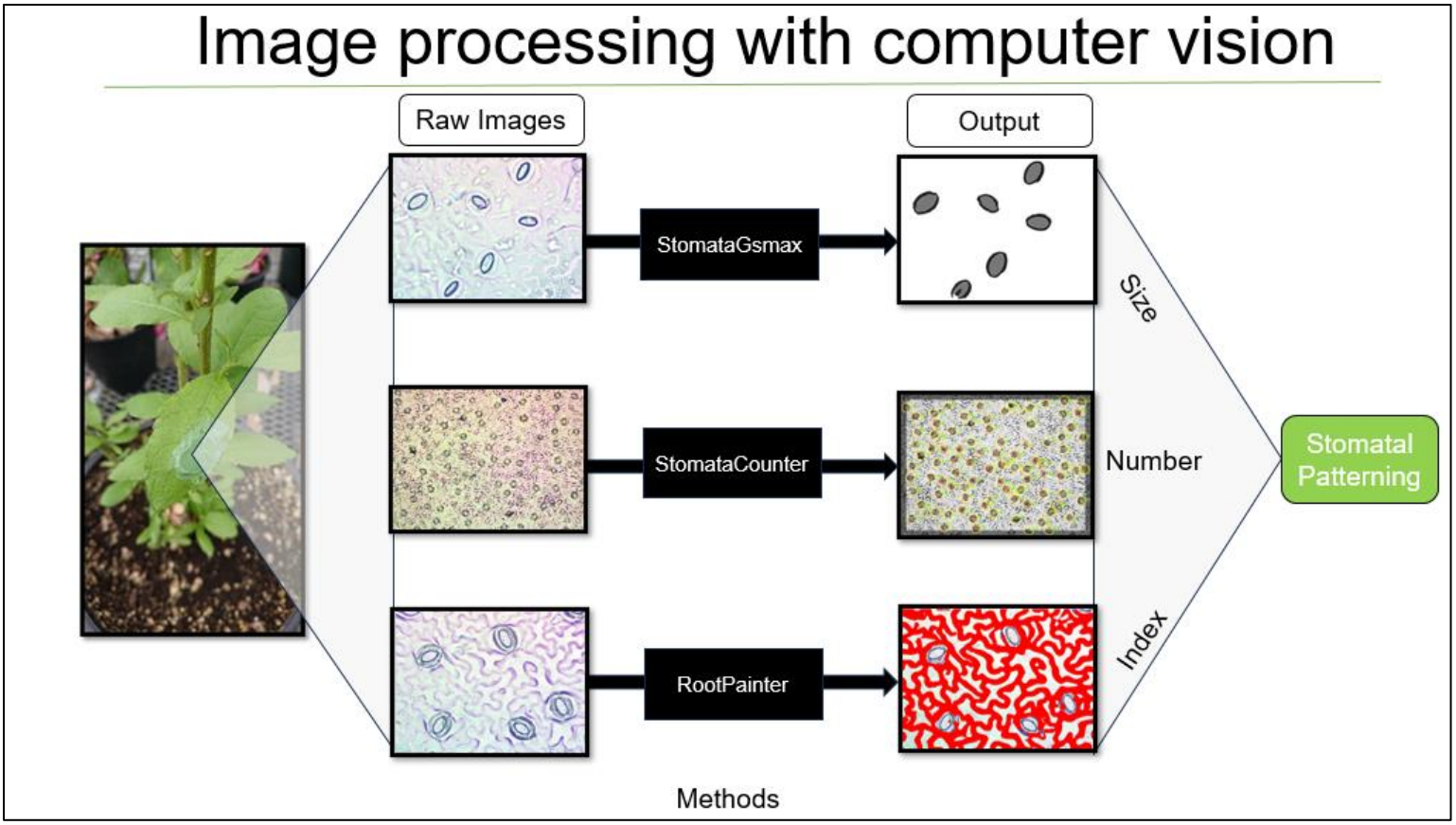

A4. Schematic representation showing the image processing to gather stomatal traits. Images of impressions were taken at 400x magnification for stomatal dimension and index data, and 100x for density. Convolutional neural network models were trained and validated from StomataGSmax (Gibbs et al., 2021) for automating morphological measurements and RootPainter (Smith et al. 2022) and StomataCounter (Fetter et al., 2019), to assist manual counting of cells. Any manual measurements were performed in ImageJ. Future efforts can likely focus on only using StomataGSmax due to its accuracy and capability to collect multiple types of data simultaneously.

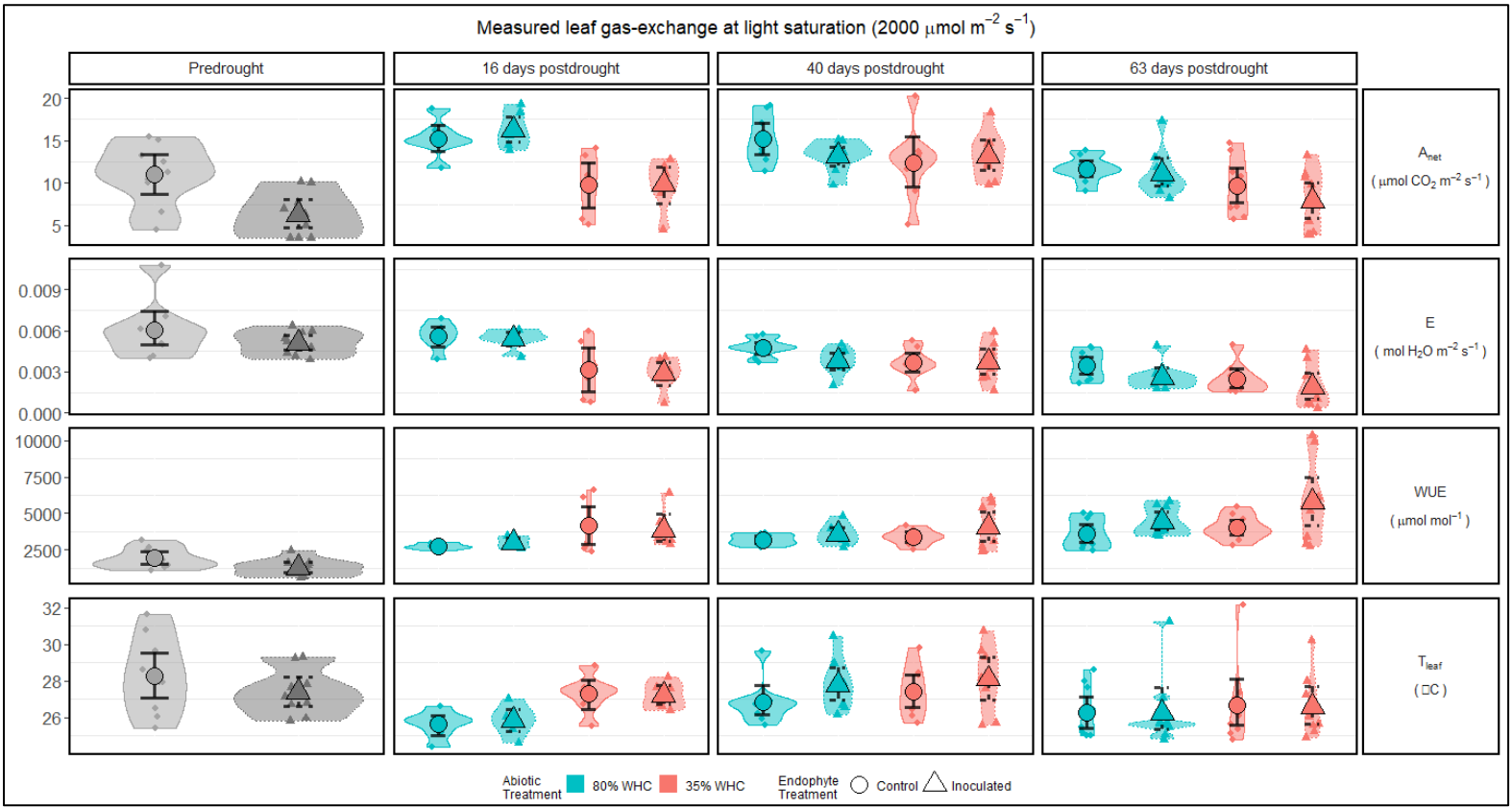

A5. Violin plots of leaf-gas exchange taken at light saturation (2000 μmol photons m^{-2} s^{-1}) from the youngest, fully expanded leaf of uninoculated (control; circles) and endophyte-inoculated (triangles) *Populus trichocarpa* pre (shaded) and post water-deficit. Blue represents well-watered (80% WHC) and red illustrates water-deficit (35%) soil-moisture conditions. Enlarged shapes represent the mean and lines illustrate the 95% confidence intervals of the net assimilation rate (A_{net}), leaf transpiration (*E*), and extrinsic water-use efficiency (WUE), and leaf temperature (T_{leaf}). Confidence intervals were created from the quantiles of case-resampled bootstrap replicates (n = 1000).

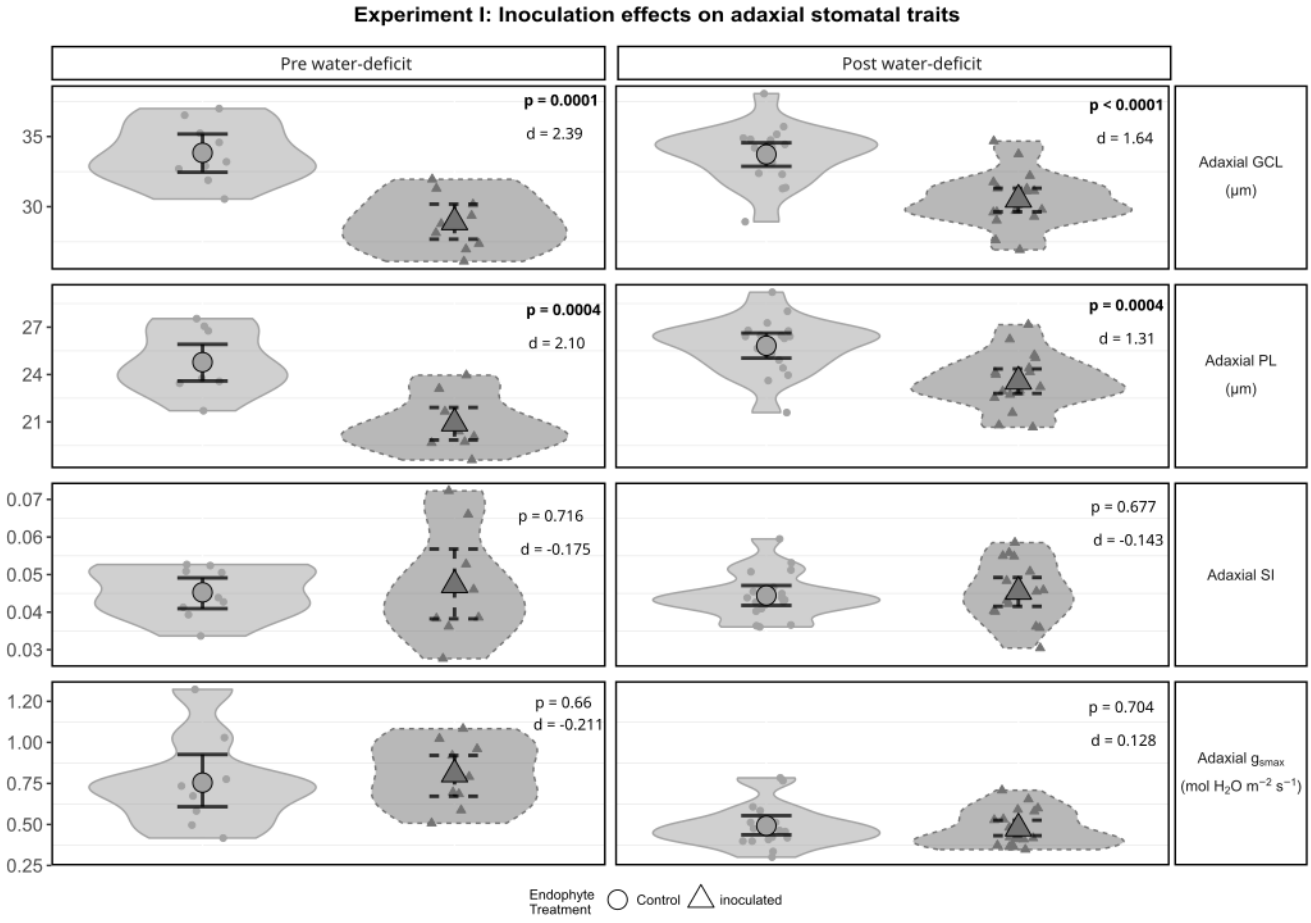

A6. Experiment I: main effect plots of adaxial stomatal anatomy from uninoculated (control; circles) and endophyte-inoculated (triangles) *Populus trichocarpa* pre and post water-deficit. Enlarged shapes represent the mean and lines illustrate the ±95% confidence interval of guard cell length (GCL), pore length (PL), stomatal index (SI), and anatomical maximum stomatal conductance (g_{smax}). Cohen's d effect sizes shown for comparisons of inoculation treatments to express the magnitude of mean differences. Confidence intervals were created from the quantiles of case-resampled bootstrap replicates (n = 1000).

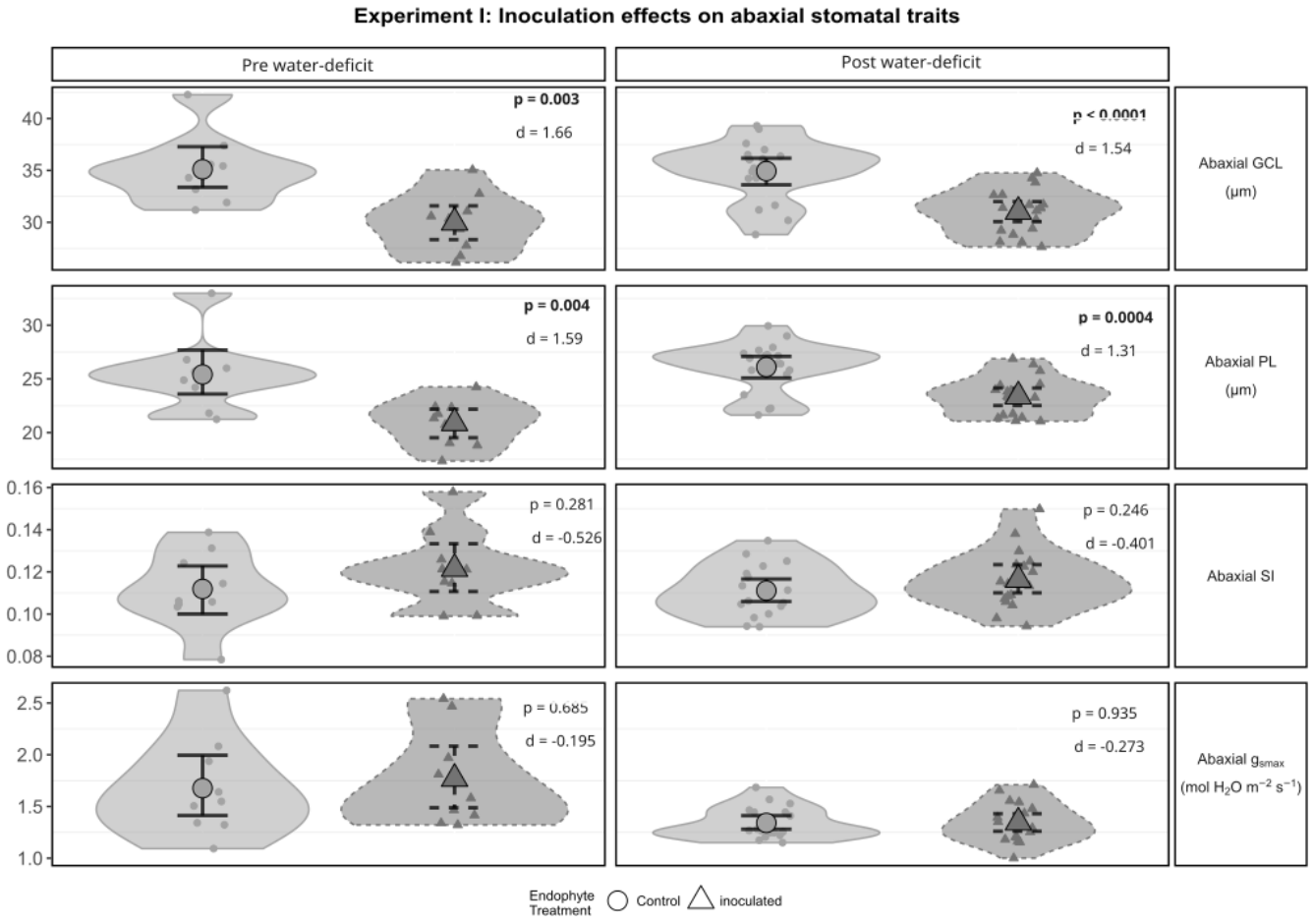

A7. Experiment I: main effect plots of abaxial stomatal anatomy from uninoculated (control; circles) and endophyte-inoculated (triangles) *Populus trichocarpa* pre and post water-deficit. Enlarged shapes represent the mean and lines illustrate the ±95% confidence interval of guard cell length (GCL), pore length (PL), stomatal index (SI), and anatomical maximum stomatal conductance (g_{smax}). Cohen's d effect sizes shown for comparisons of inoculation treatments to express the magnitude of mean differences Confidence intervals were created from the quantiles of case-resampled bootstrap replicates (n = 1000).

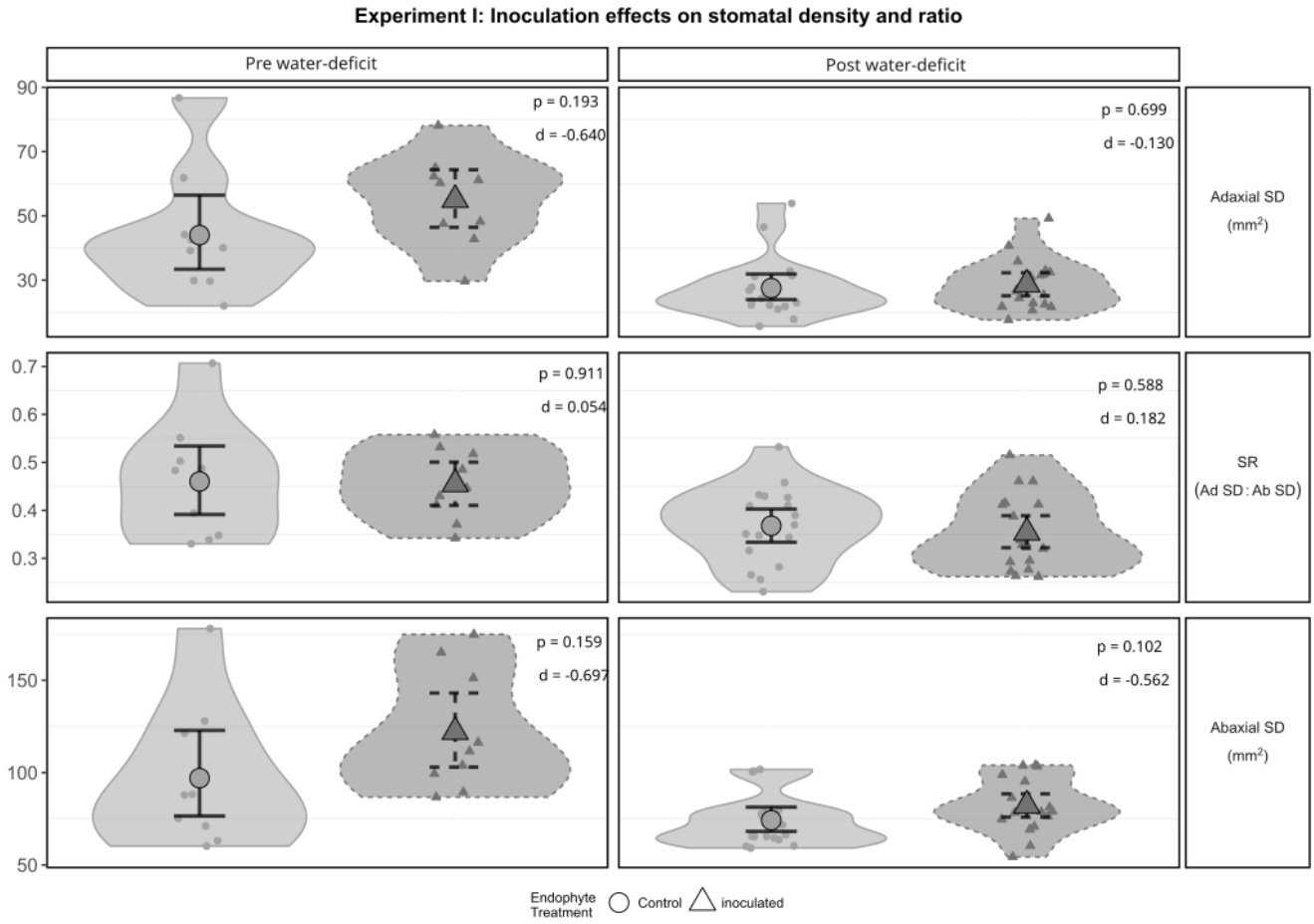

A8. Experiment I: main effect plots of adaxial (top row) and abaxial (bottom row) stomatal densities (SD), and their ratios (SR; middle row) from uninoculated (control; circles) and endophyte-inoculated (triangles) *Populus trichocarpa* pre and post water-deficit. Enlarged shapes represent the mean and lines illustrate the ±95% confidence interval of stomatal density (SD) and stomatal ratio (SR). Cohen's d effect sizes shown for comparisons of inoculation treatments to express the magnitude of mean differences. Confidence intervals were created from the quantiles of case-resampled bootstrap replicates (n = 1000).

A9. Experiment I: effect sizes (adj η_p^2) of each treatment for the examined traits before and after water-stress. Significant terms ($\alpha = 0.05$) are bolded and based on non-parametric ANOVA models (see Methods and Results). For both adaxial (Ad) and abaxial (Ab) leaf surfaces, examined traits include guard cell length (GCL; µm), pore length (PL; µm), pore width (PW; µm), maximum anatomical stomatal conductance (g_{smax}; mol m^{-2} s^{-1}), stomatal density (SD; mm^{-2}), stomatal index (SI), and stomatal density ratio (SR). Values labeled with '*' had marginal significance ($p < 0.1$)

	GCL		PL		PW		g_{smax}		SD		SI		SR
	Ad	Ab	Ad	Ab	Ad	Ab	Ad	Ab	Ad	Ab	Ad	Ab	
Treatment	Pre-water-deficit												
Inoculation	**0.59**	**0.40**	**0.53**	**0.38**	0	**0.17**	0	0	0.05	0.07	0	0.01	0
	Post water-deficit												
Inoculation	**0.22**	**0.23**	**0.15**	**0.17**	0	0.01	0	0	0	0.03*	0	0.01	0
Water-deficit	0.03*	**0.12**	0.01	**0.12**	0	**0.17**	**0.13**	0	**0.13**	0.01	0.01	0	**0.08**
Inoculation x Water-deficit	0	0	0.01	0	**0.03**	0.01	0	0	0	0.01	0.02	0	0.01
Time	0.03*	0	**0.04**	0.01	0.01	**0.25**	**0.17**	0.01	**0.14**	0	0.01	0.03*	**0.23**
Inoculation x Time	0.04*	0	0.01	0	0	0	0	0	0	0	0.02	0	0
Water-deficit x Time	0	0	0	0	0	**0.04**	0.01	0.03*	0.02	0.02	0.01	**0**	0.02

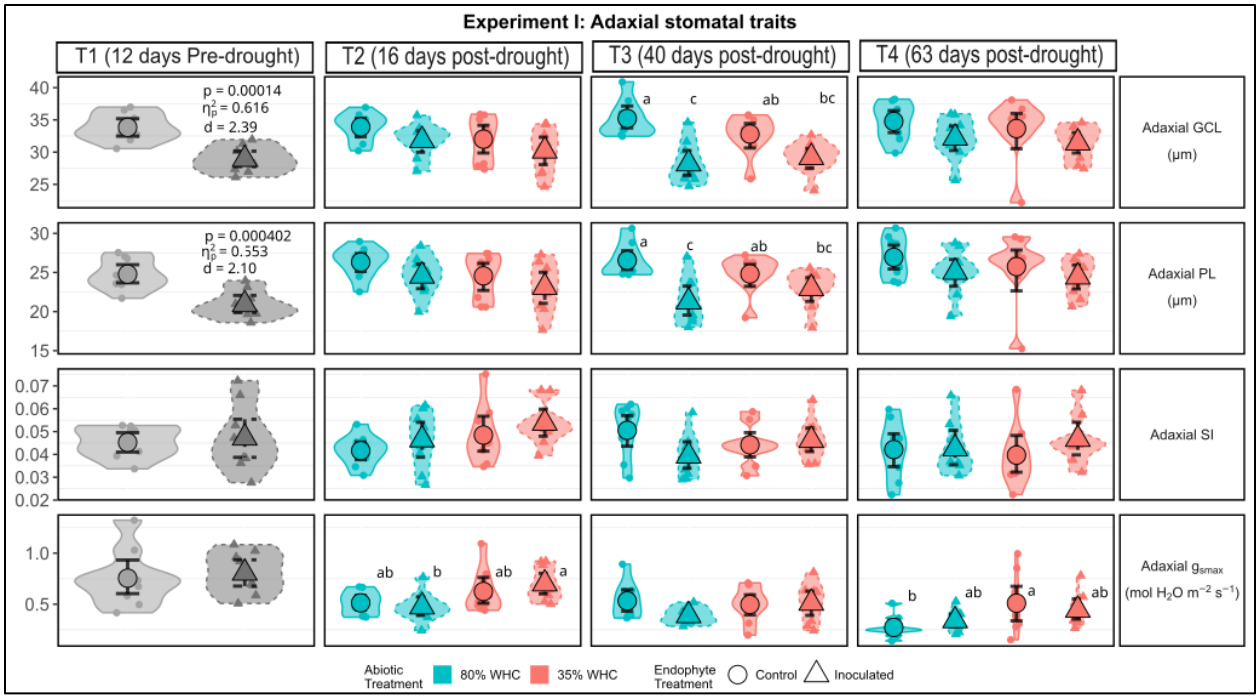

A10. Experiment I: violin plots of adaxial stomatal anatomy from uninoculated (control; circles) and endophyte-inoculated (triangles) *Populus trichocarpa* for each sampling timepoint. Blue represents well-watered (80% WHC) and red illustrates water-deficit (35%) soil-moisture conditions. Enlarged shapes represent the mean and lines illustrate the ±95% confidence interval of guard cell length (GCL), pore length (PL), stomatal index (SI), and anatomical maximum stomatal conductance (g_{smax}). Partial eta squared and Cohen's d effect sizes shown for comparisons of inoculation treatments before water-stress. Compact letter display (CLD) used to represent significant differences ($P < 0.05$) between treatment means, using the results of Wilcoxon-Mann-Whitney *post-hoc* tests. Confidence intervals were created from the quantiles of case-resampled bootstrap replicates (n = 1000).

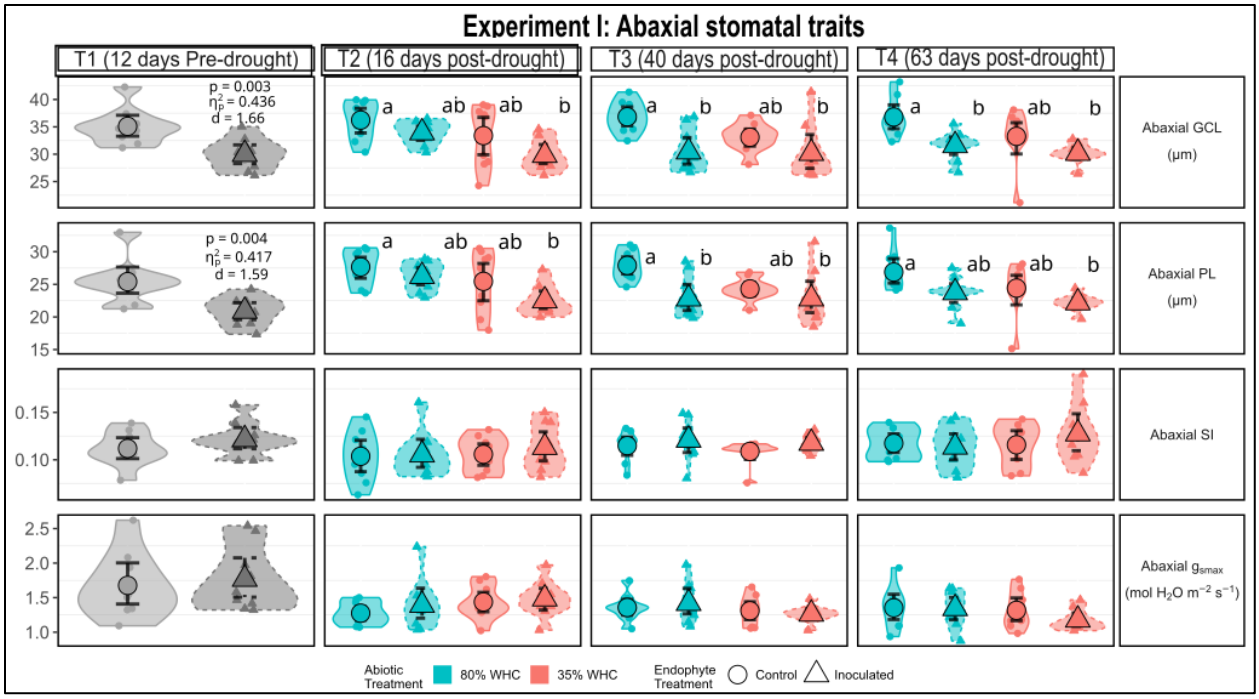

A11. Experiment I: violin plots of abaxial stomatal anatomy from uninoculated (control; circles) and endophyte-inoculated (triangles) *Populus trichocarpa* for each sampling timepoint. Blue represents well-watered (80% WHC) and red illustrates water-deficit (35%) soil-moisture conditions. Enlarged shapes represent the mean and lines illustrate the ±95% confidence interval of guard cell length (GCL), pore length (PL), stomatal index (SI), and anatomical maximum stomatal conductance (g_{smax}). Partial eta squared and Cohen's d shown for comparisons of inoculation treatments before water-stress. Compact letter display (CLD) used to represent significant differences ($P < 0.05$) between treatment means, using the results of Wilcoxon-Mann-Whitney *post-hoc* tests. Confidence intervals were created from the quantiles of case-resampled bootstrap replicates (n = 1000).

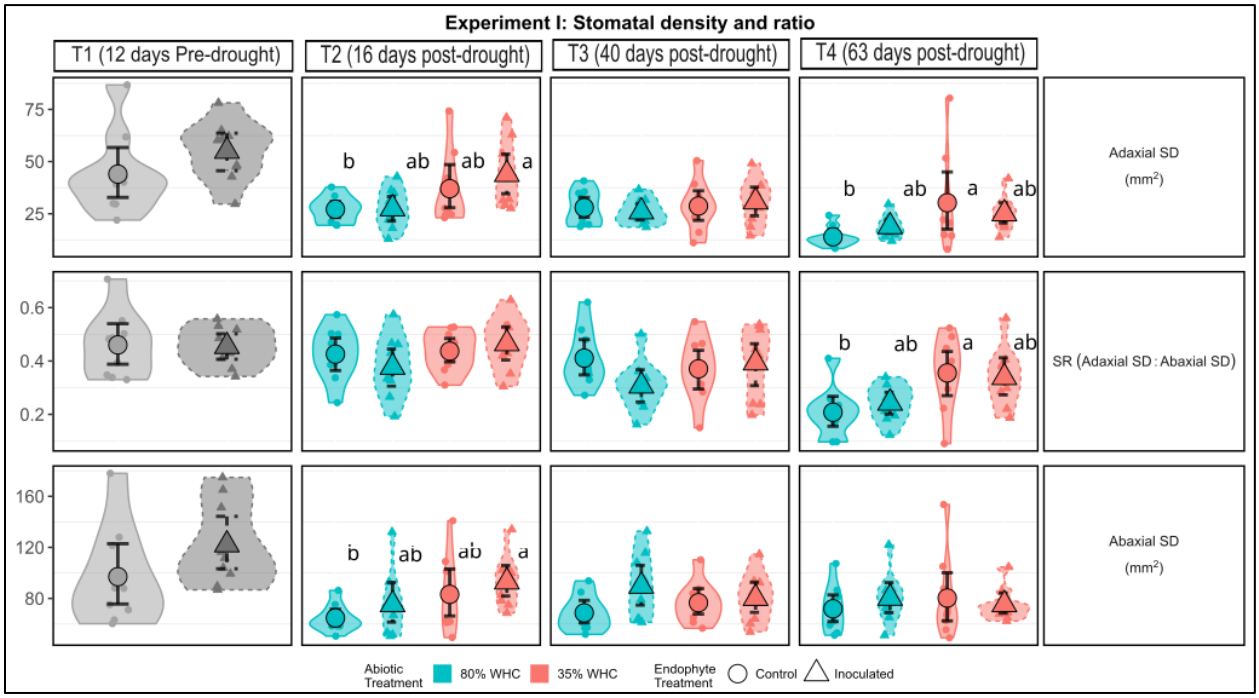

A12. Experiment I: violin plots of adaxial (top row) and abaxial (bottom row) stomatal densities (SD), and their ratios (SR; middle row) from uninoculated (control; circles) and endophyte-inoculated (triangles) *Populus trichocarpa* for each sampling timepoint. Blue represents well-watered (80% WHC) and red illustrates water-deficit (35%) soil-moisture conditions. Enlarged shapes represent the mean and lines illustrate the ±95% confidence interval of stomatal density (SD) and stomatal ratio (SR). Compact letter display (CLD) used to represent significant differences ($P < 0.05$) between treatment means, using the results of Wilcoxon-Mann-Whitney *post-hoc* tests. Confidence intervals were created from the quantiles of case-resampled bootstrap replicates (n = 1000).

A13. Experiment I: PERMANOVA tables before and after water-stress, showing the effects of inoculation, water-deficit, and their interaction. Only a subset (n = 18) of the sample plants were examined prior to water-deficit. Post water-deficit examined all available plants (n = 32) by aggregating values from sampling timepoints 2- 4. Significant values are bolded at (α = 0.05).

	Pre-water-deficit					*Post water-deficit*				
	DF	SS	R^2	F	p	DF	SS	R^2	F	p
Block	4	3.92	0.25	-	-	8	4.63	0.19	-	-
Inoculation	1	3.28	0.21	4.56	**0.007**	1	3.39	0.14	5.02	**0.004**
Water-deficit	-	-	-	-	-	1	3.30	0.13	4.88	**0.01**
Interaction	-	-	-	-	-	1	0.68	0.03	1.01	0.37
Residual	12	8.60	0.54	-	-	19	12.84	0.52	-	-
Total	17	15.78	1.00	-	-	30	24.84	1.00	-	-

A14. Experiment I: PERMANOVA tables from each timepoint examining the effects of inoculation, water-deficit, and their interaction on stomatal patterning. Timepoint 1 (Baseline) examined only a subset of the total available samples (n = 18) and Timepoints 2- 4 included each sample (n = 36). Significant values are bolded at (α = 0.05).

	Timepoint 1					*Timepoint 2*					*Timepoint 3*					*Timepoint 4*				
	DF	SS	R^2	F	p	DF	SS	R^2	F	p	DF	SS	R^2	F	p	DF	SS	R^2	F	p
Block	4	3.92	0.25	-	-	8	7.85	0.27	-	-	8	5.84	0.20	-	-	8	4.13	0.23	-	-
Inoculation	1	3.28	0.21	4.56	**0.007**	1	1.44	0.05	2.19	0.09	1	3.64	0.13	5.31	**0.001**	1	0.68	0.04	1.24	0.28
Water deficit	-	-	-	-	-	1	3.65	0.13	5.57	**0.01**	1	1.48	0.05	2.17	0.08	1	2.31	0.13	4.23	**0.001**
Interaction	-	-	-	-	-	1	0.51	0.02	0.78	0.47	1	1.51	0.05	2.21	0.07	1	0.68	0.04	1.24	0.28
Residual	12	8.60	0.54	-	-	24	15.72	0.54	-	-	24	16.43	0.57	-	-	19	10.37	0.57	-	-
Total	17	15.78	1.00	-	-	35	29.16	1.00	-	-	35	28.90	1.00	-	-	30	18.16	1.00	-	-

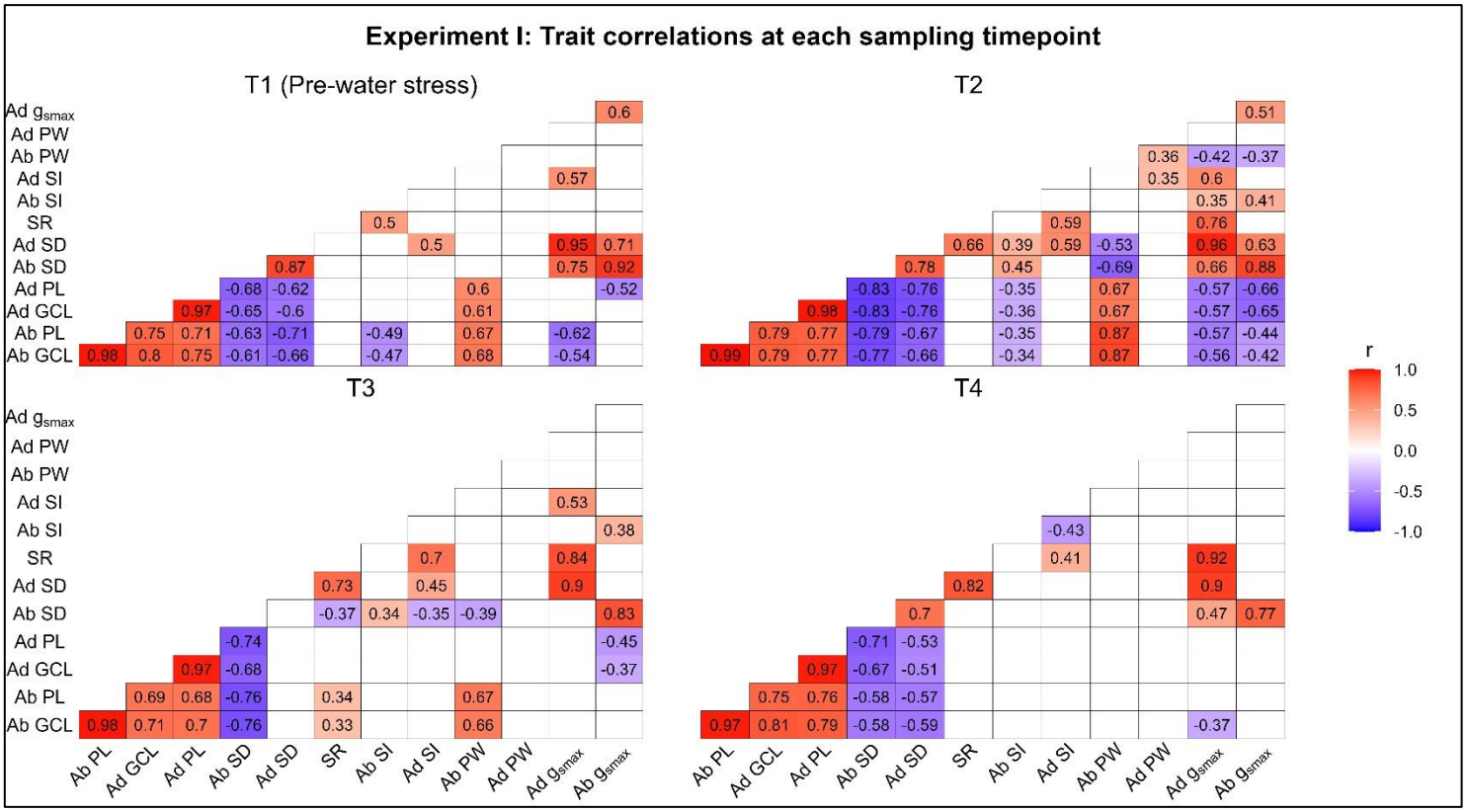

A15. Experiment I: matrices representing the correlations between each stomatal variable. Pearson's correlation coefficient (r) is shown for each significant relationship ($p < 0.05$) along with either red or blue colors indicating positive or negative correspondence, respectively. Blank cells represent nonsignificant correlations. For both adaxial (Ad) and abaxial (Ab) leaf surfaces, examined traits include guard cell length (GCL), pore length (PL), pore width (PW), stomatal index (SI), anatomical maximum stomatal conductance (g_{smax}) stomatal density (SD), and stomatal density ratio (SR).

A16. Loading tables generated from the principal component analysis before and after water-stress. Only a subset (n = 18) of the sample plants were examined prior to water-deficit. Post water-deficit examined all available plants (n = 32) by aggregating values from timepoints 2- 4. Loadings were bolded if their magnitude was greater than 0.3, and these were considered the as the main traits a part of a principal component.

	Pre-water-deficit		*Post water-deficit*	
Response Variable	PC1	PC2	PC1	PC2
Abaxial GCL	**0.340**	0.232	**0.360**	0.113
Abaxial PL	**0.348**	0.214	**0.361**	0.104
Adaxial GCL	**0.328**	0.108	**0.352**	0.145
Adaxial PL	**0.324**	0.052	**0.353**	0.161
Abaxial SD	**-0.341**	**0.304**	**-0.357**	-0.172
Adaxial SD	**-0.362**	0.109	**-0.332**	**0.322**
SR	-0.070	**-0.416**	-0.161	**0.556**
Abaxial SI	-0.198	**-0.301**	-0.129	-0.148
Adaxial SI	-0.166	0.177	-0.041	**0.480**
Abaxial PW	0.250	0.264	**0.308**	0.056
Adaxial PW	-0.081	**0.417**	0.017	0.105
Adaxial g_{smax}	**-0.314**	0.100	-0.263	**0.425**
Abaxial g_{smax}	-0.255	**0.482**	-0.211	-0.201
Proportion of Variance Explained	0.491	0.160	0.472	0.194
Cumulative Variance Explained	0.491	0.651	0.472	0.666

A17. Experiment I: loading tables generated during the Principal Component Analysis at each timepoint. Loadings were bolded if their magnitude was greater than 0.3, and these were considered the main traits a part of a principal component.

	Timepoint 1		*Timepoint 2*		*Timepoint 3*		*Timepoint 4*	
Response Variable	PC1	PC2	PC1	PC2	PC1	PC2	PC1	PC2
Abaxial GCL	**0.340**	0.232	**0.326**	0.208	**0.395**	0.074	**0.376**	0.103
Abaxial PL	**0.348**	0.214	**0.329**	0.214	**0.391**	0.063	**0.365**	0.111
Adaxial GCL	**0.328**	0.108	**0.340**	0.112	**0.367**	0.008	**0.363**	0.231
Adaxial PL	**0.324**	0.052	**0.339**	0.099	**0.379**	-0.007	**0.368**	0.233
Abaxial SD	**-0.341**	**0.304**	**-0.345**	-0.098	**-0.407**	-0.083	**-0.363**	-0.175
Adaxial SD	**-0.362**	0.109	**-0.342**	0.234	-0.083	**-0.547**	**-0.381**	0.244
SR	-0.070	**-0.416**	-0.142	**0.478**	0.207	**-0.473**	-0.247	**0.487**
Abaxial SI	-0.198	**-0.301**	-0.180	0.107	-0.120	-0.089	-0.016	**-0.366**
Adaxial SI	-0.166	0.177	-0.162	**0.472**	0.196	**-0.358**	-0.016	**0.457**
Abaxial PW	0.250	0.264	0.285	**0.306**	0.232	0.118	0.087	-0.031
Adaxial PW	-0.081	**0.417**	0.005	**0.407**	-0.113	-0.109	0.006	0.033
Adaxial g_{smax}	**-0.314**	0.100	**-0.301**	**0.319**	0.070	**-0.540**	-0.291	**0.415**
Abaxial g_{smax}	-0.255	**0.482**	-0.262	-0.023	-0.268	-0.081	-0.162	-0.160
Proportion of Variance Explained	0.491	0.160	0.546	0.172	0.396	0.237	0.401	0.186
Cumulative Variance Explained	0.491	0.651	0.546	0.718	0.396	0.633	0.401	0.587

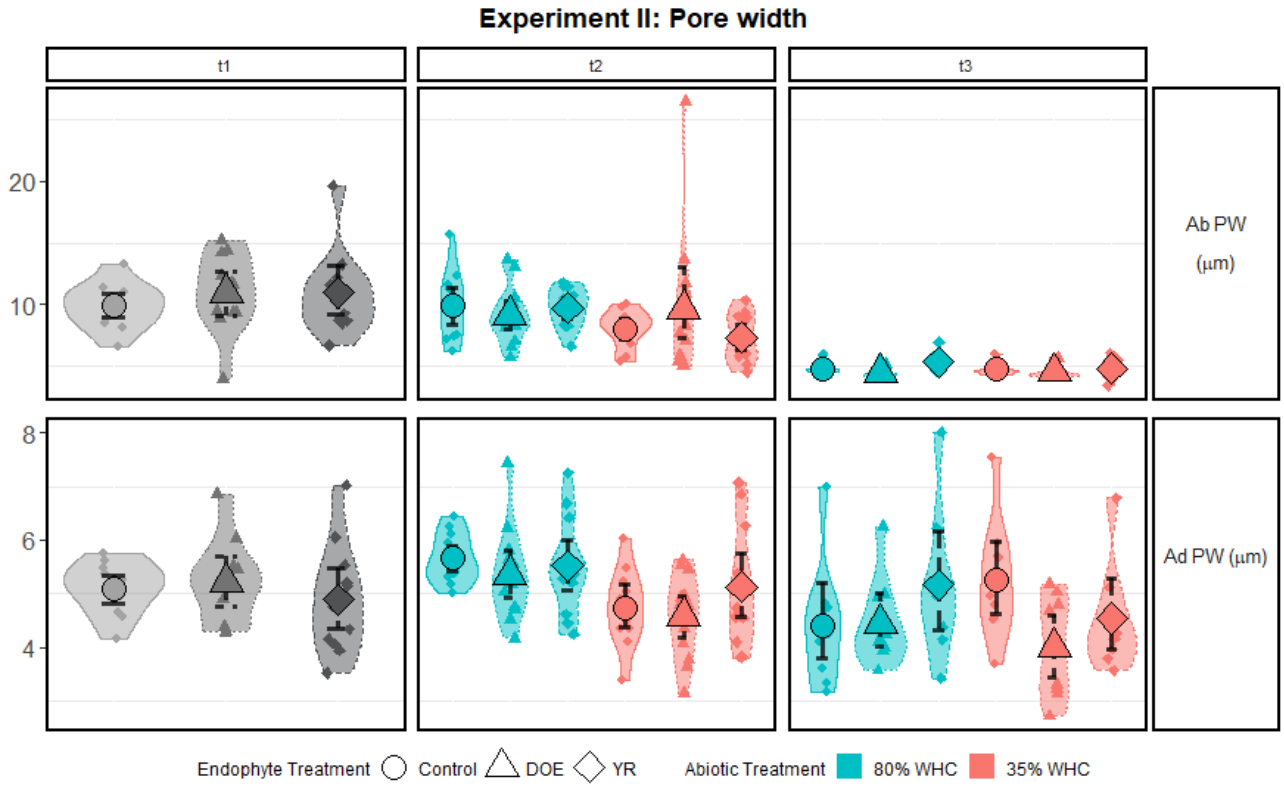

A18. Experiment II: violin plots of abaxial (top row) and adaxial (bottom row) stomatal pore widths (PW) from uninoculated (control; circles) and endophyte-inoculated (triangles) *Populus trichocarpa* for each sampling timepoint. Blue represents well-watered (80% WHC) and red illustrates water-deficit (35%) soil-moisture conditions. Enlarged shapes represent the mean and lines illustrate the ±95% confidence intervals. Compact letter display (CLD) used to represent significant differences ($P < 0.05$) between treatment means, using the results of *Wilcoxon-Mann-Whitney post-hoc* tests. Confidence intervals were created from the quantiles of case-resampled bootstrap replicates (n = 1000).